

## **Supplementary Materials for “GCAP 2.0: A global 3-D chemical-transport model for past, present and future climate scenarios”**

**Lee T. Murray<sup>1,2</sup>, Eric M. Leibensperger<sup>3</sup>, Clara Orbe<sup>4</sup>, Loretta J. Mickley<sup>5</sup>, and Melissa Sulprizio<sup>5</sup>**

<sup>1</sup>Dept. of Earth & Environmental Sciences, University of Rochester, Rochester, NY USA

<sup>2</sup>Dept. of Physics & Astronomy, University of Rochester, Rochester, NY USA

<sup>3</sup>Dept. of Physics & Astronomy, Ithaca College, Ithaca, NY USA

<sup>4</sup>NASA Goddard Institute for Space Studies, New York, NY USA

<sup>5</sup>School of Engineering and Applied Sciences, Harvard University, Cambridge, MA USA

**Correspondance:** Lee T. Murray (lee.murray@rochester.edu)

### **Contents**

<b>S1 Meteorology</b>	<b>S-2</b>
<b>S2 Emissions</b>	<b>S-53</b>
<b>S3 Evaluation</b>	<b>S-62</b>

## S1 Meteorology

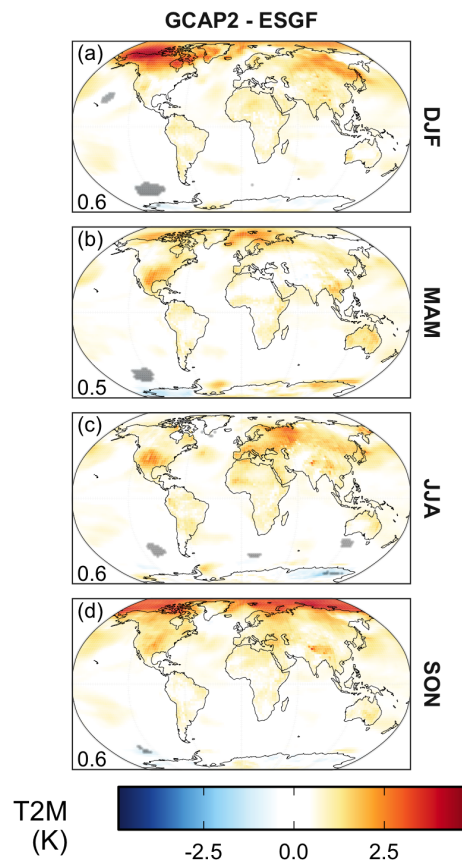


**Figure S1:** Difference in seasonal mean surface temperature (in K) in our repeat simulation with respect to the original r1i1p1f2 variant. Rows from top to bottom show the 14-year seasonal average for 2001-2014 C.E. for December-January-February (DJF), March-April-May (MAM), June-July-August (JJA), and September-October-November (SON). Gray dots indicate locations where the E2.1 simulations are statistically different with respect to interannual variability ( $p$ -value  $< 0.05$ ;  $n = 14$  yr). The number in the bottom left gives the global mean value.



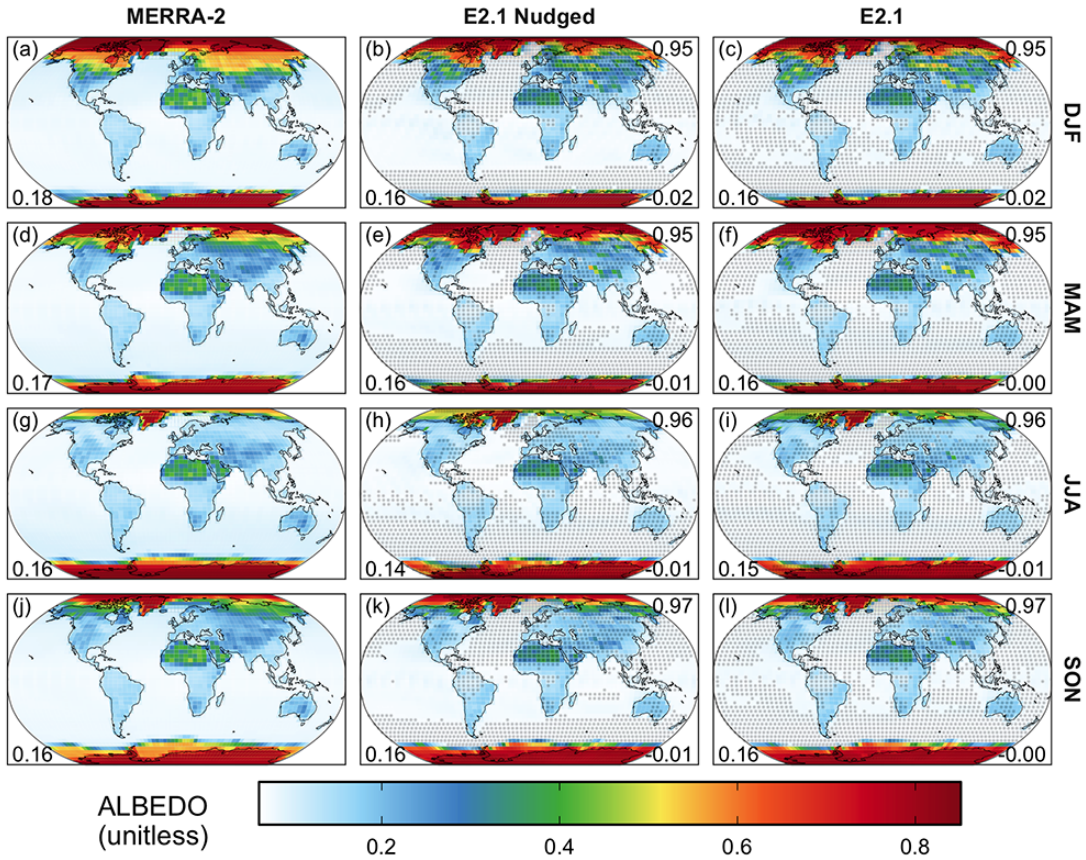


**Figure S2:** Seasonal mean climatology of the surface broadband albedo (unitless; variable name: ALBEDO). Rows from top to bottom show the 10-year seasonal average for 2005-2014 C.E. for December-January-February (DJF), March-April-May (MAM), June-July-August (JJA), and September-October-November (SON). Columns from left to right show the values from the MERRA-2 reanalysis (Gelaro et al., 2017), E2.1 nudged to MERRA-2, and the free-running E2.1. All products have been horizontally re-gridded to a common  $4^\circ$  latitude by  $5^\circ$  longitude resolution for comparison. Gray dots indicate locations where the E2.1 simulations are statistically different with respect to interannual variability ( $p$ -value  $< 0.05$ ;  $n = 10$  yr). The number in the bottom left gives the global mean value. The number in the top right of the E2.1 panels gives the pattern correlation ( $R$ ) between the E2.1 runs and MERRA-2. The number in the bottom right of the E2.1 panels gives the mean difference of the simulation with respect to its MERRA-2 equivalent.

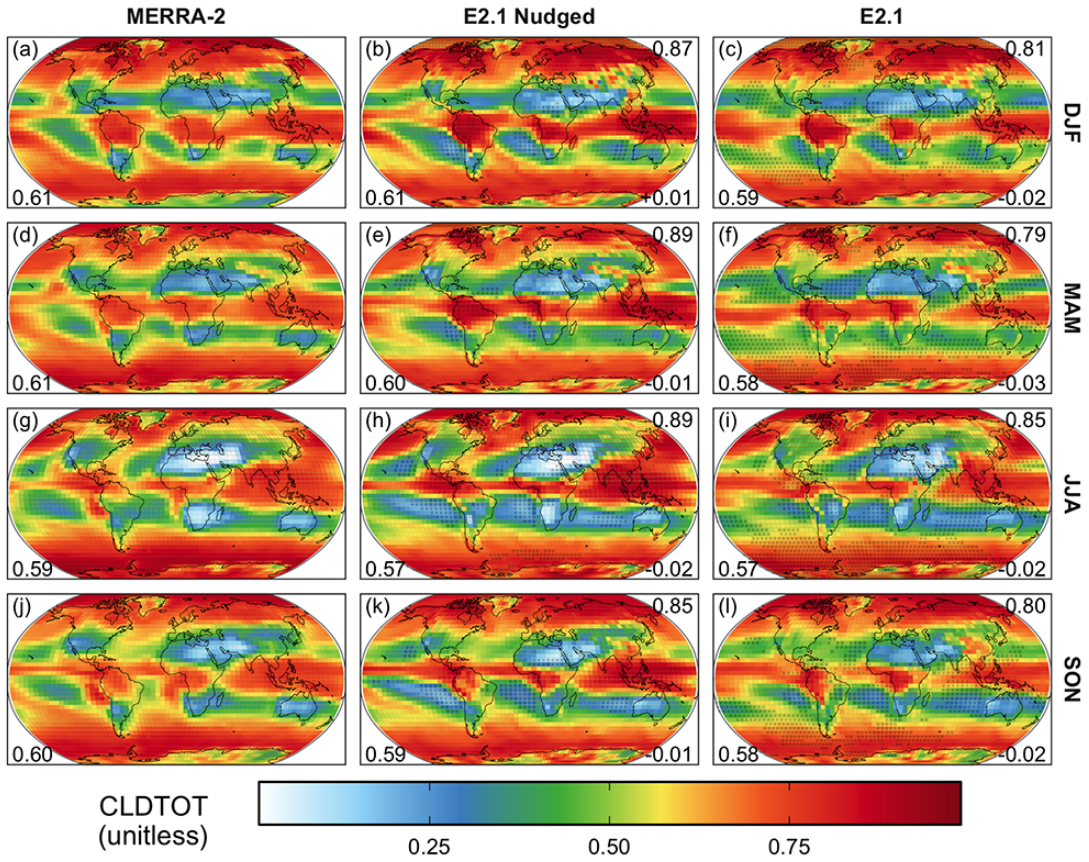


**Figure S3:** The same as Fig. S2, but for total cloud area fraction (unitless; variable name: CLDTOT).

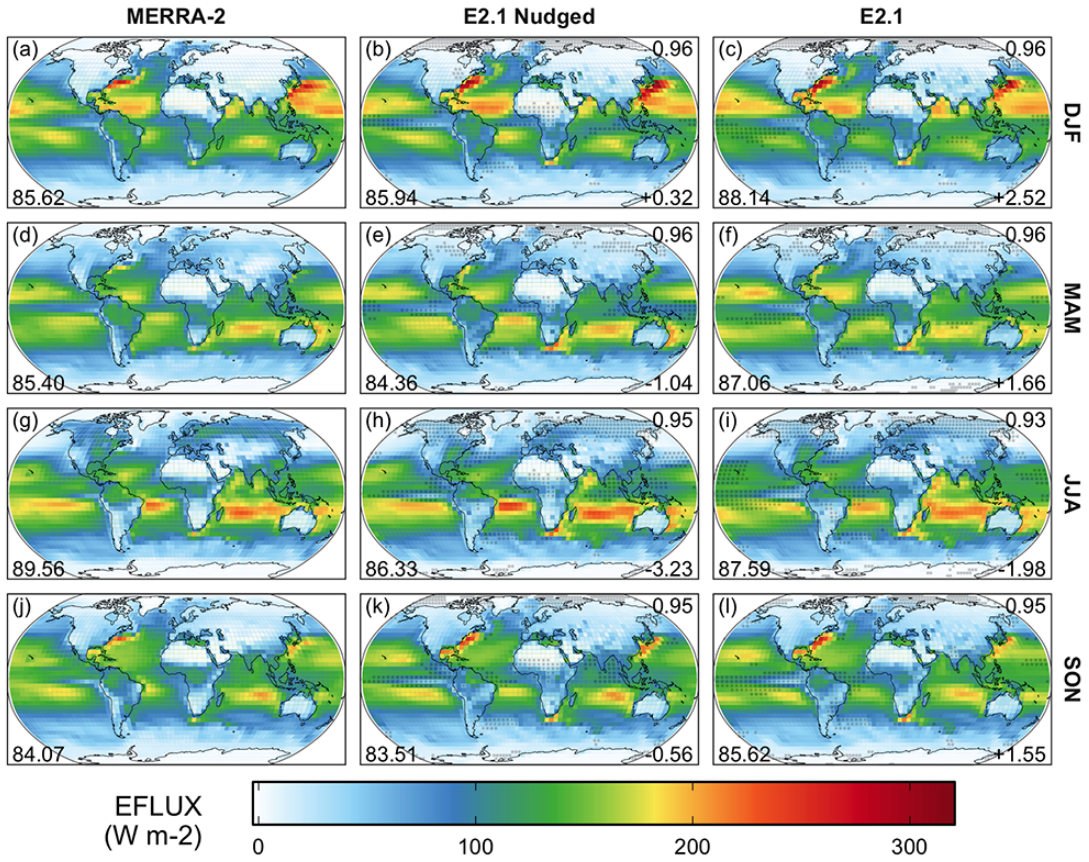


**Figure S4:** The same as Fig. S2, but for total latent energy flux (units:  $\text{W m}^{-2}$ ; variable name: EFLUX).



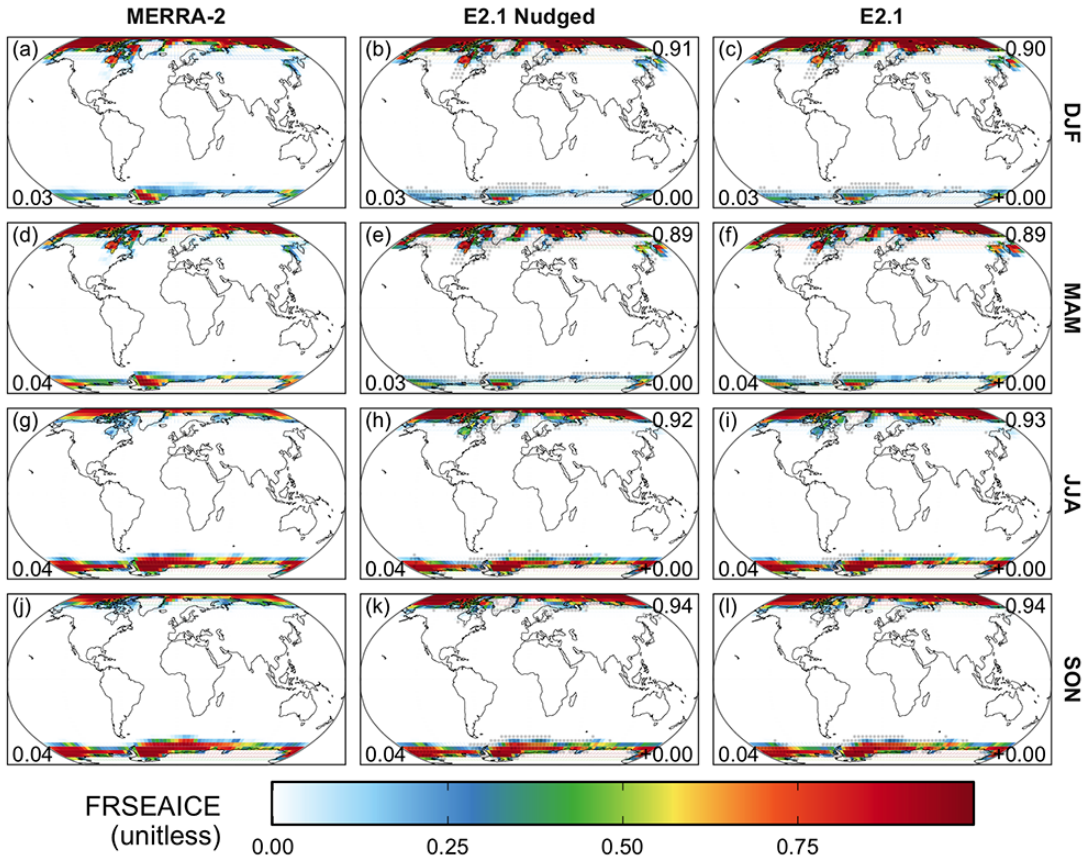


**Figure S5:** The same as Fig. S2, but for fraction of sea ice (unitless; variable name: FRSEAIce).

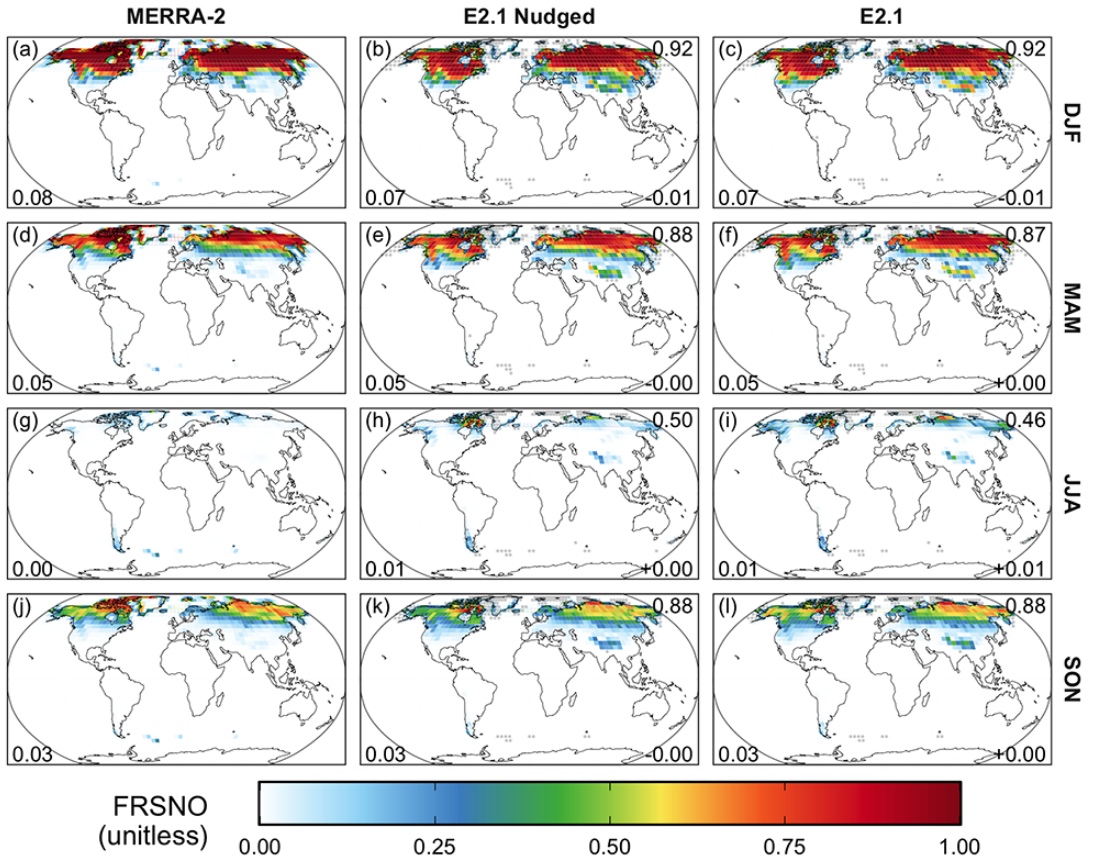


**Figure S6:** The same as Fig. S2, but for fraction of snow coverage on land (unitless; variable name: FRSNO).

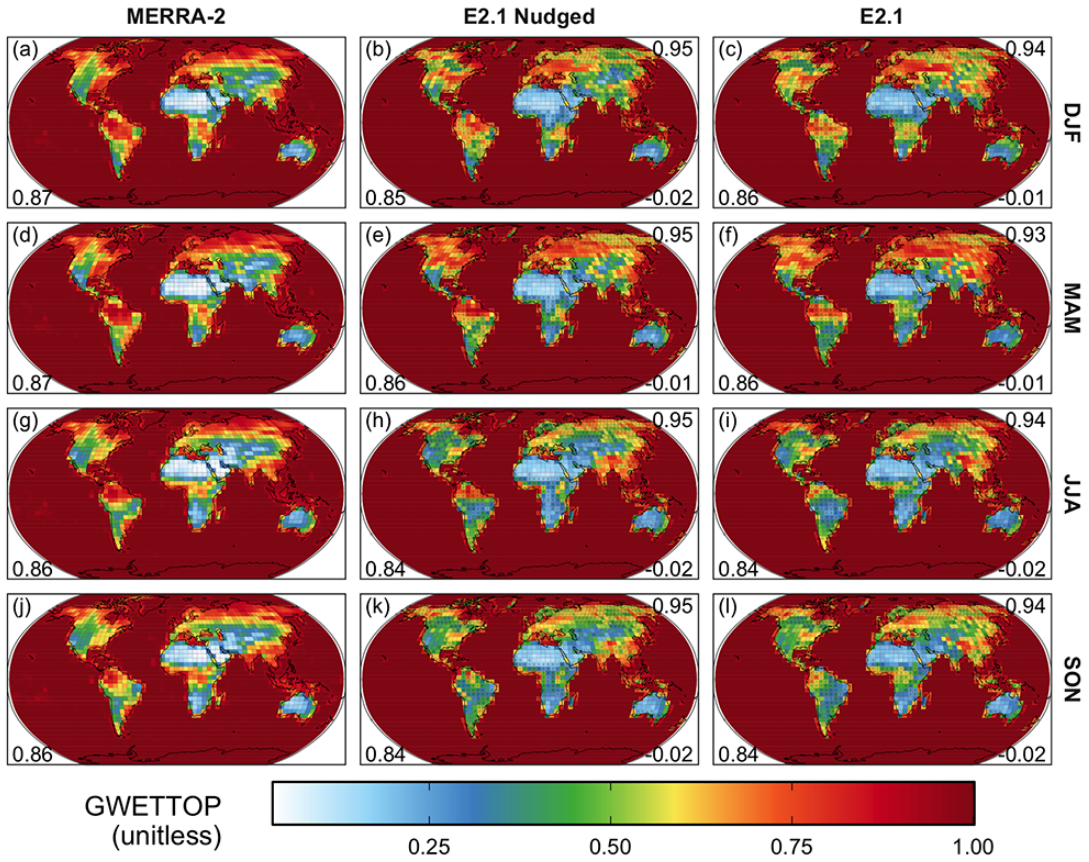


**Figure S7:** The same as Fig. S2, but for surface soil wetness (unitless; variable name: GWETTOP).

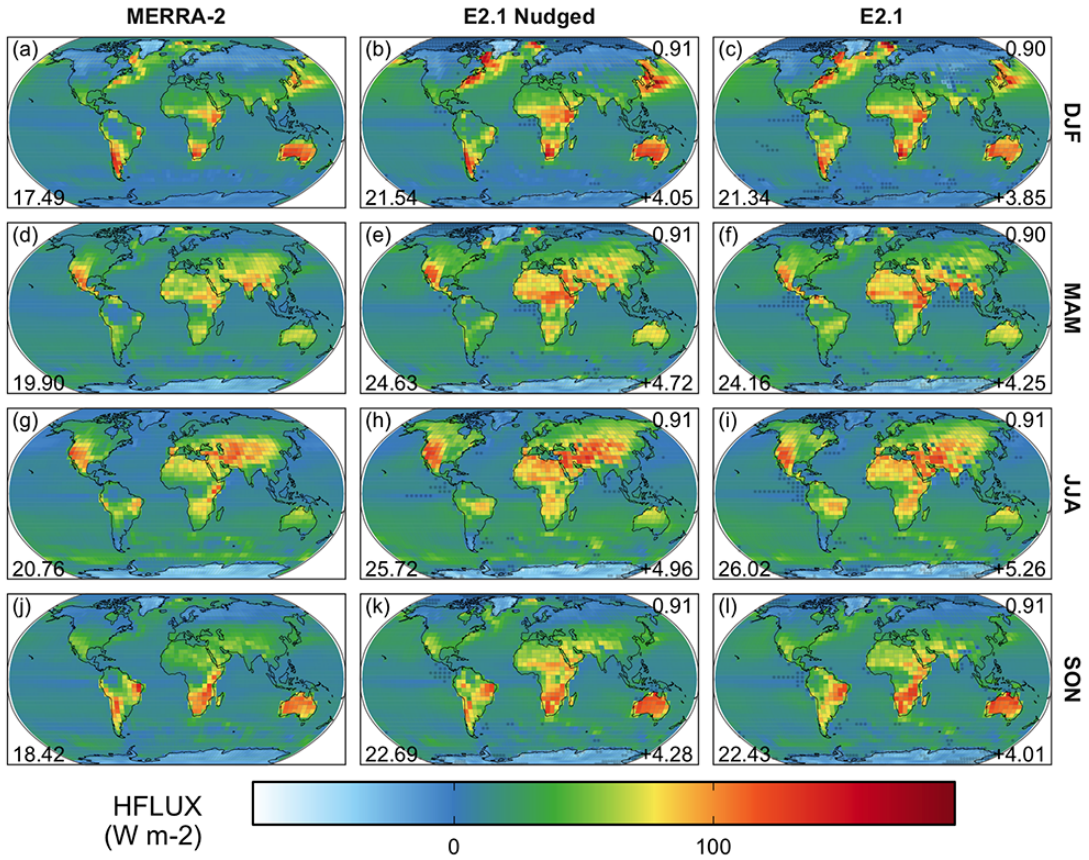


**Figure S8:** The same as Fig. S2, but for surface sensible heat flux from turbulence (units:  $\text{W m}^{-2}$ ; variable name: HFLUX).



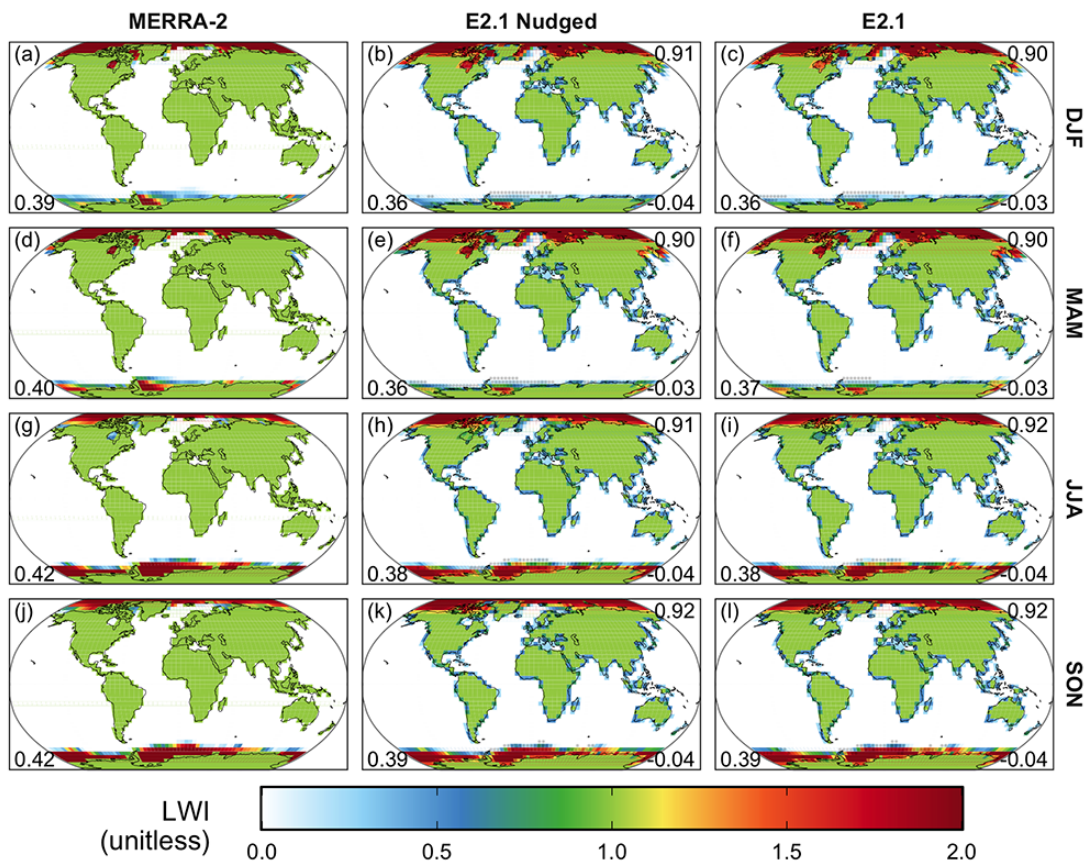


**Figure S9:** The same as Fig. S2, but for water (0), land (1), or ice (2) surface classification (unitless; variable name: LWI).



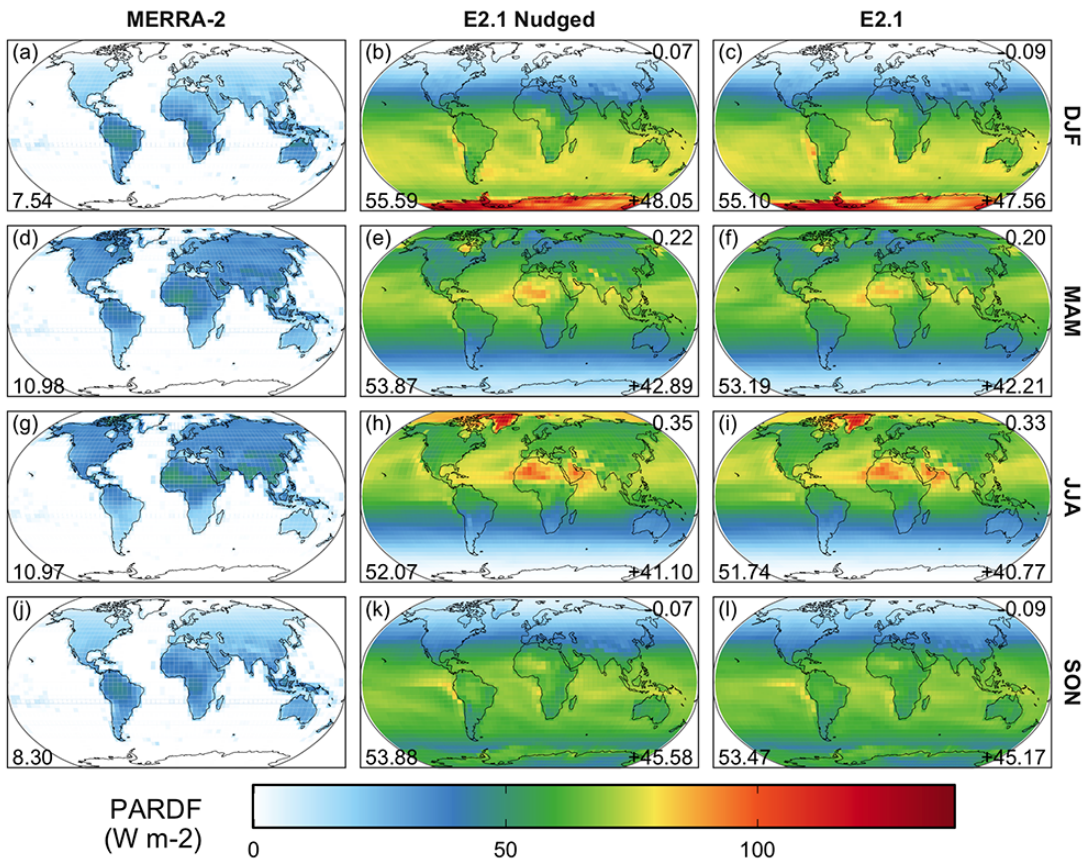


**Figure S10:** The same as Fig. S2, but for photosynthetically active diffuse downward radiation (units:  $\text{W m}^{-2}$ ; variable name: PARDF).

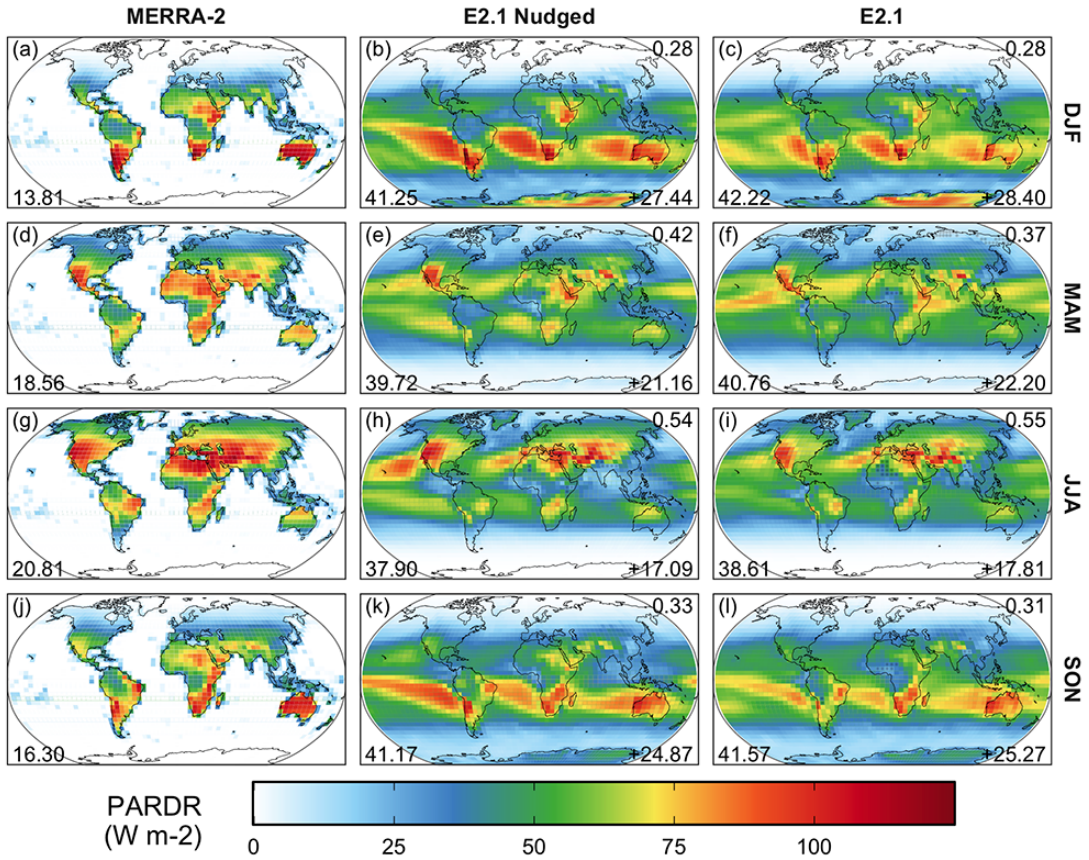


**Figure S11:** The same as Fig. S2, but for photosynthetically active direct downward radiation (units:  $\text{W m}^{-2}$ ; variable name: PARDR).

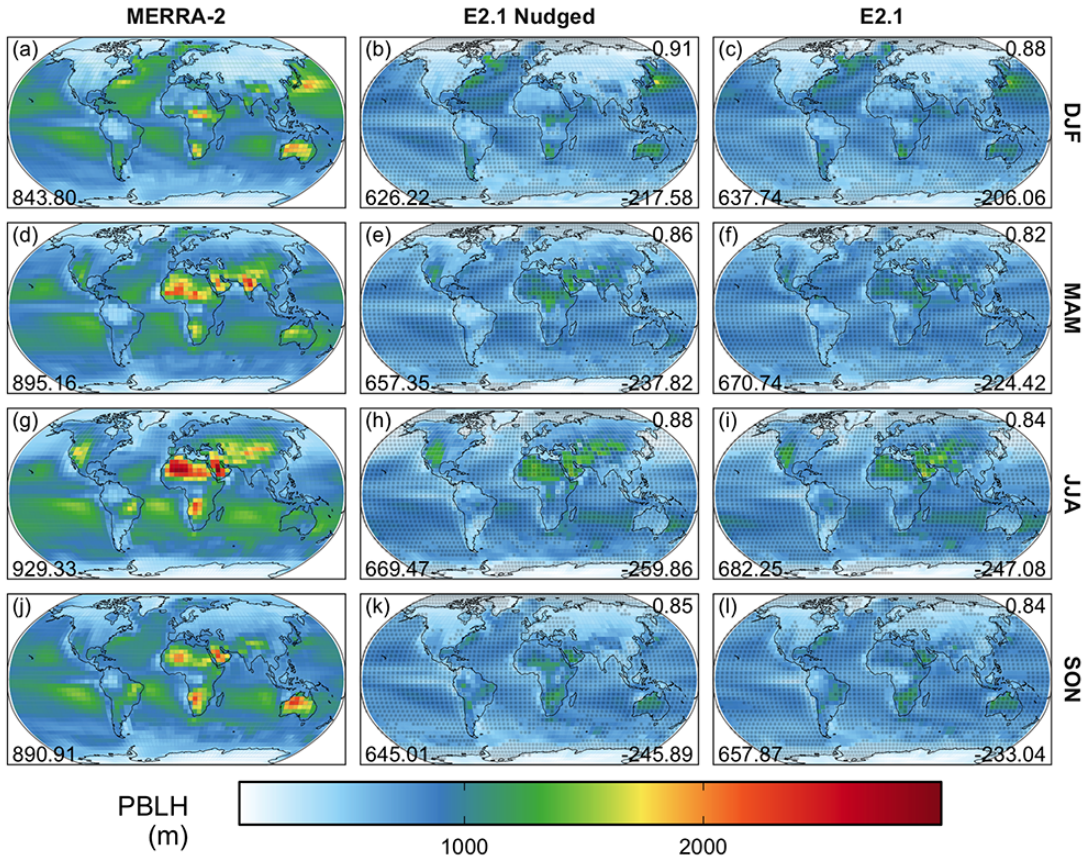


**Figure S12:** The same as Fig. S2, but for planetary boundary layer height (units: m; variable name: PBLH).



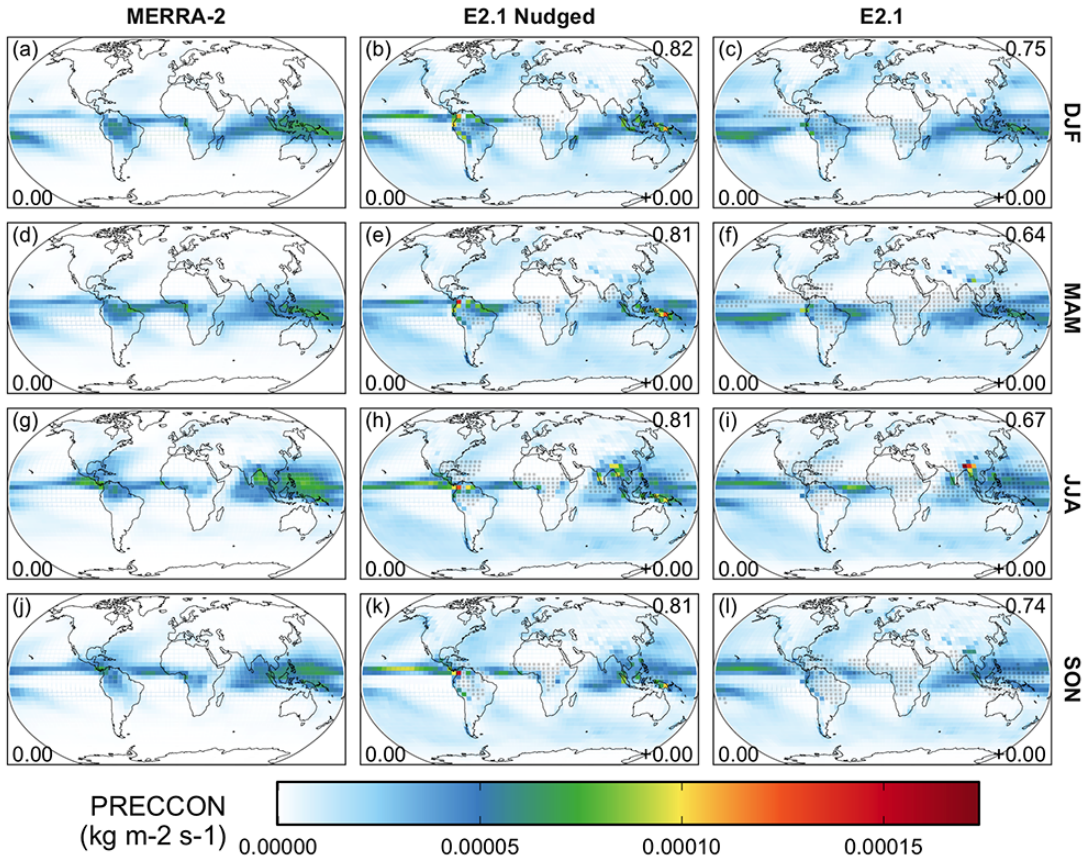


**Figure S13:** The same as Fig. S2, but for convective precipitation (units:  $\text{kg m}^{-2} \text{s}^{-1}$ ; variable name: PRECCON).

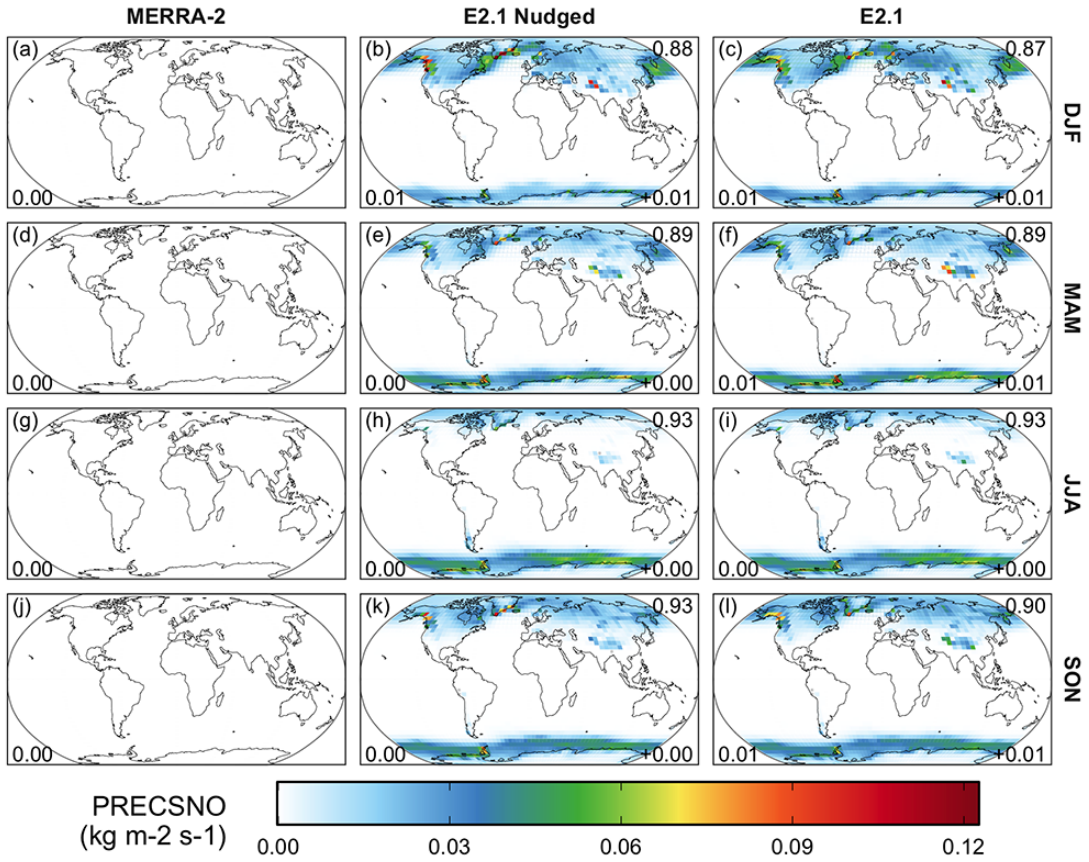


**Figure S14:** The same as Fig. S2, but for snow precipitation (units: kg m<sup>-2</sup> s<sup>-1</sup>; variable name: PRECSNO).

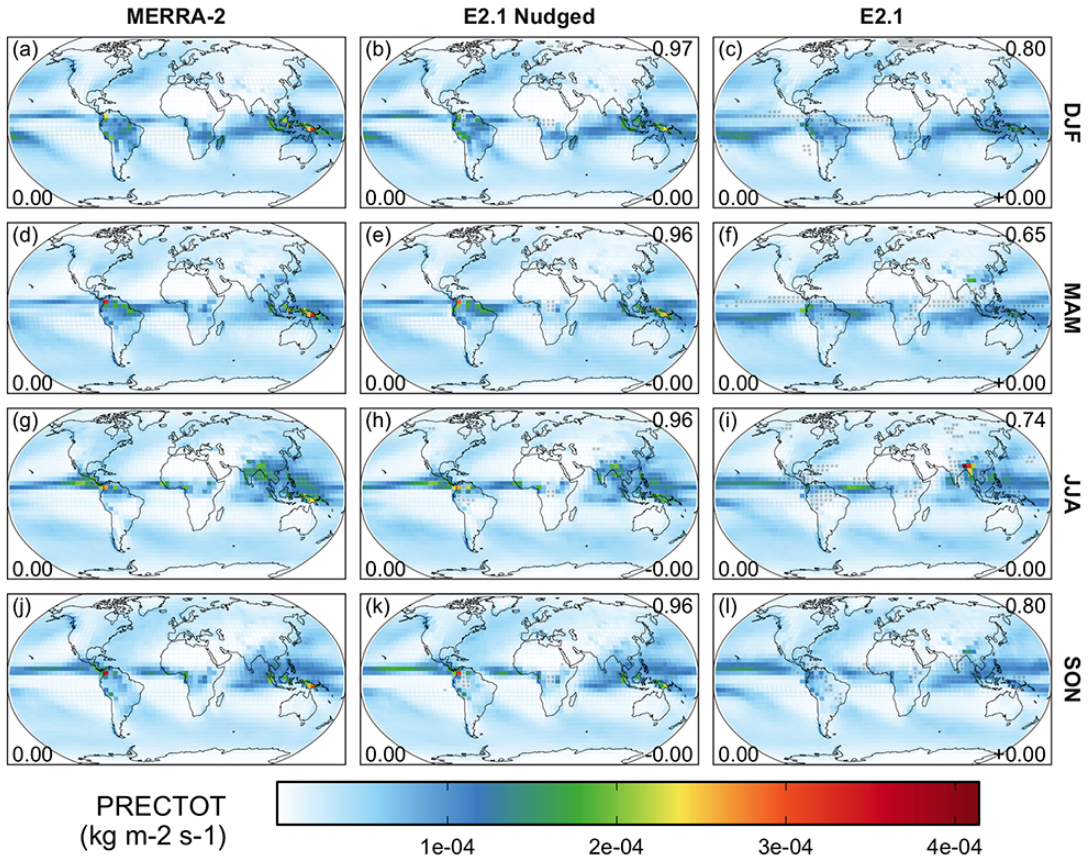


**Figure S15:** The same as Fig. S2, but for total precipitation (units:  $\text{kg m}^{-2} \text{s}^{-1}$ ; variable name: PRECTOT).

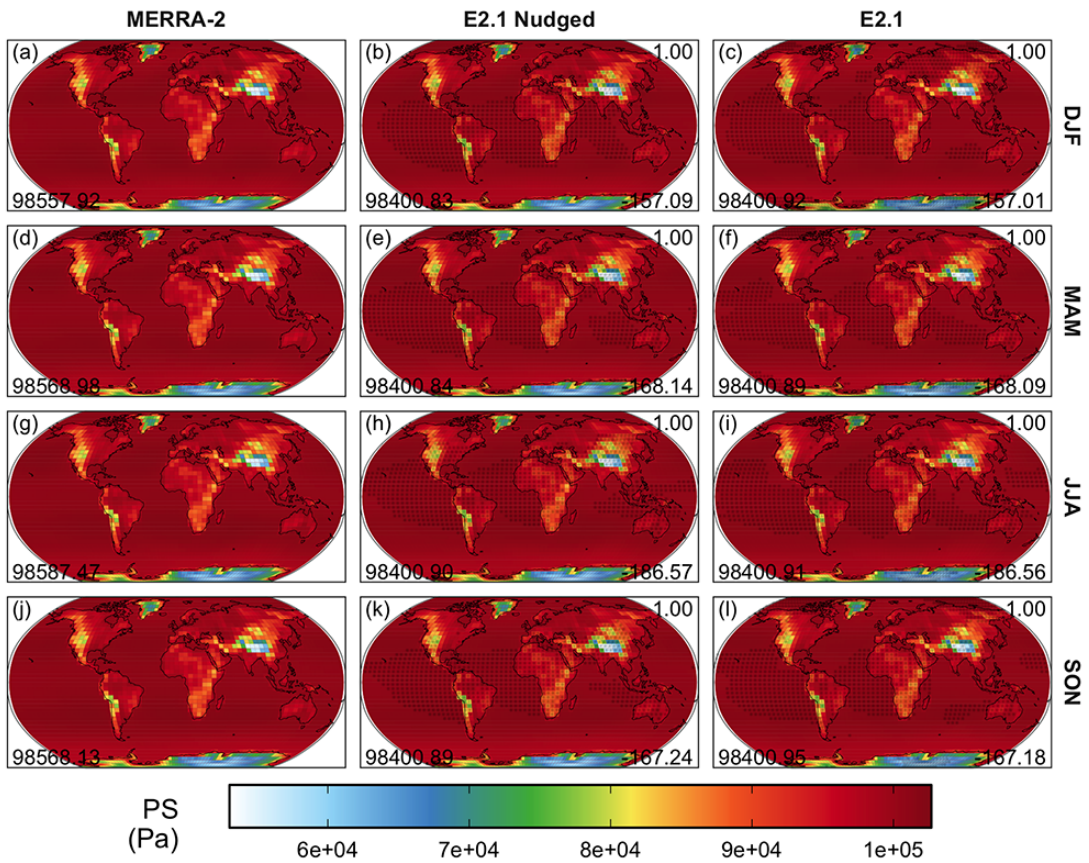


**Figure S16:** The same as Fig. S2, but for surface pressure (units: Pa; variable name: PS).



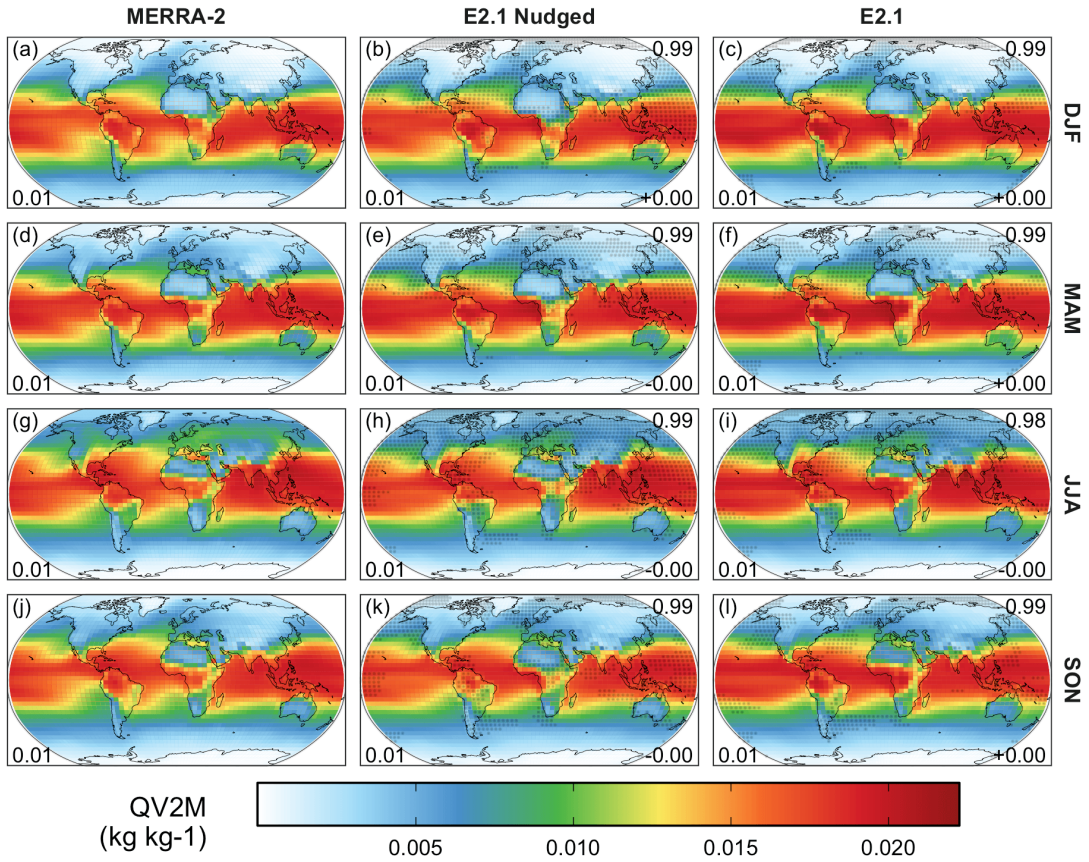


**Figure S17:** The same as Fig. S2, but for specific humidity at 2 m above the surface (units: kg kg<sup>-1</sup>; variable name: QV2M).



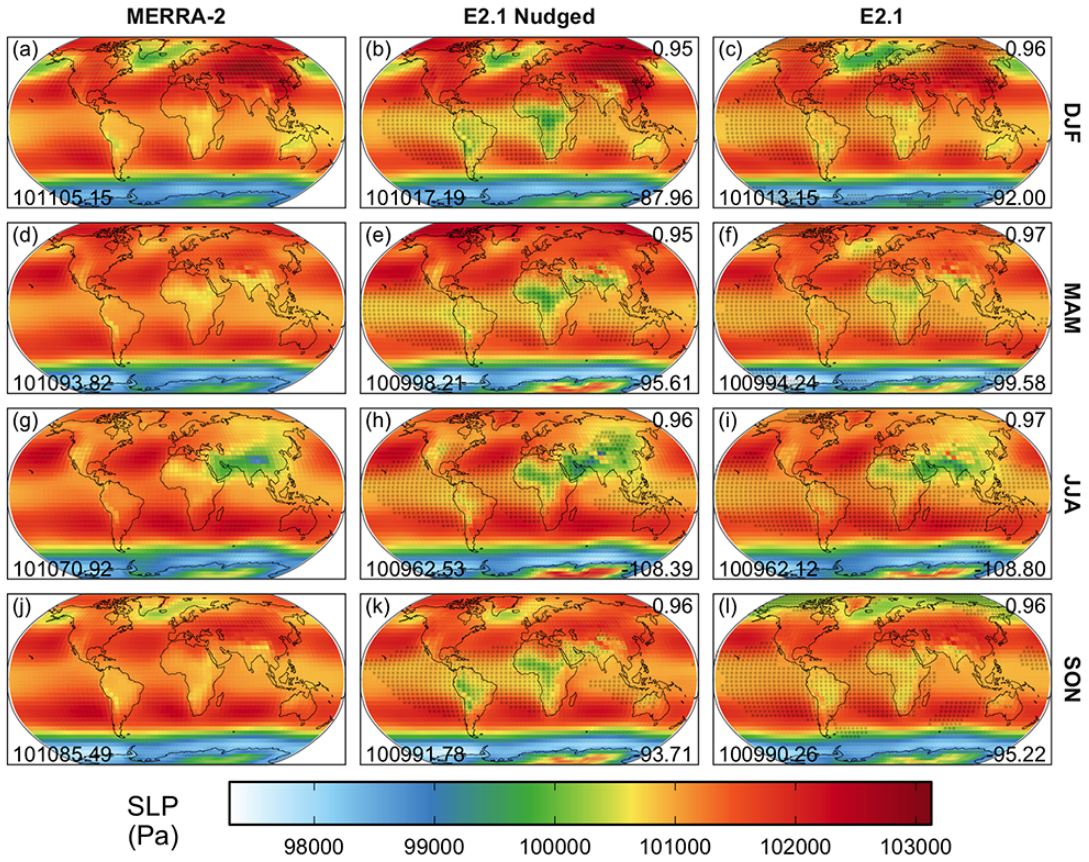


**Figure S18:** The same as Fig. S2, but for sea-level pressure (units: Pa; variable name: SLP).

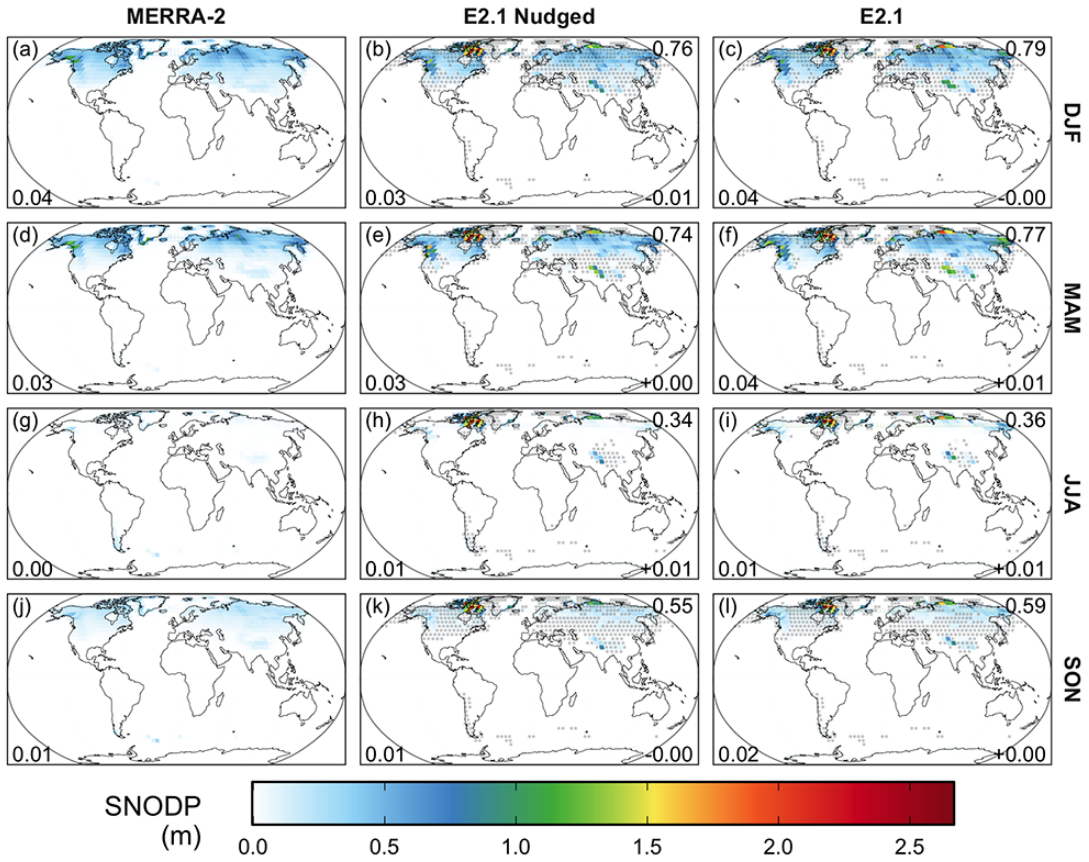


**Figure S19:** The same as Fig. S2, but for snow depth (units: m; variable name: SNODP).

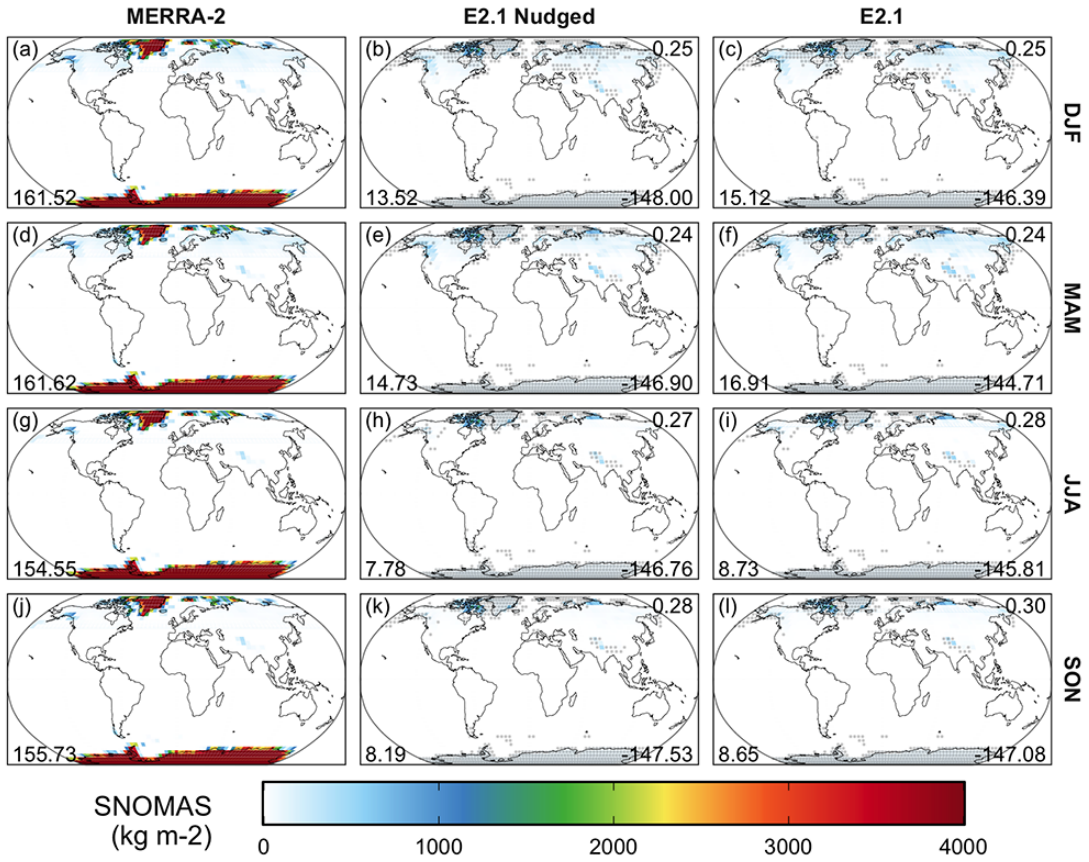


**Figure S20:** The same as Fig. S2, but for total snow storage on land (units: m; variable name: SNOMAS).

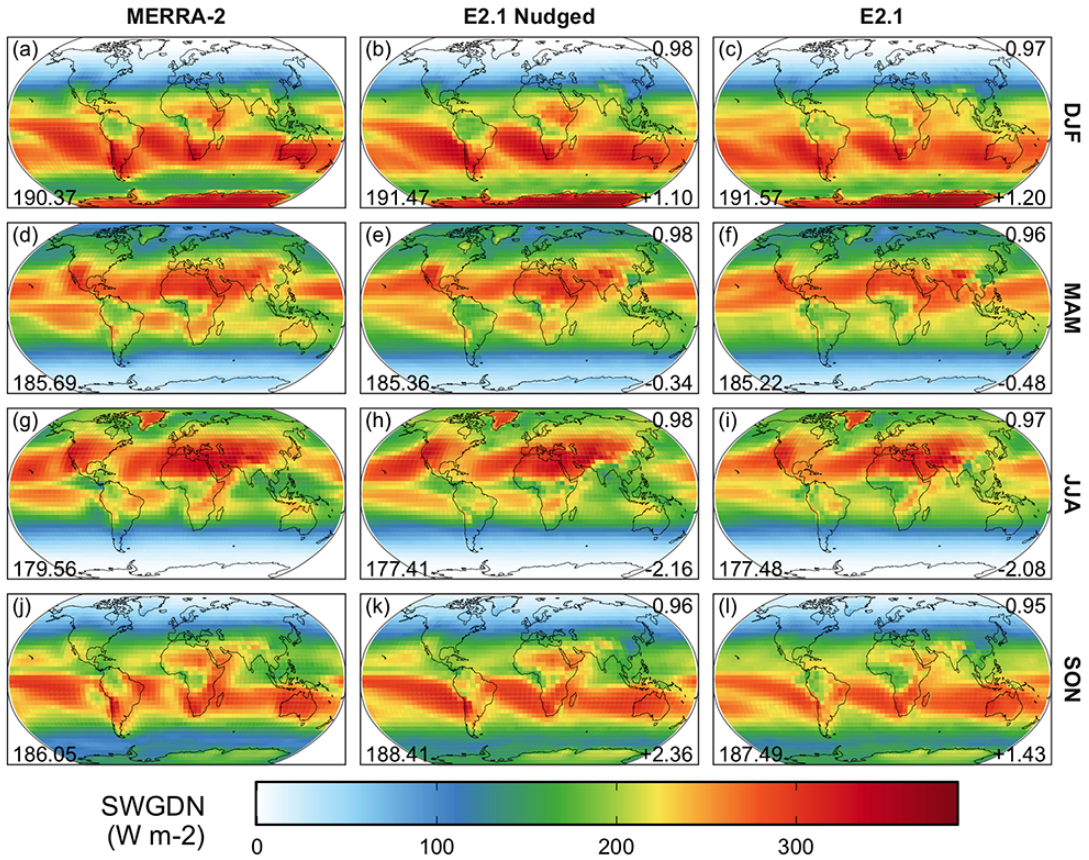


**Figure S21:** The same as Fig. S2, but for downwelling shortwave flux at the surface (units:  $\text{W m}^{-2}$ ; variable name: SWGDN).



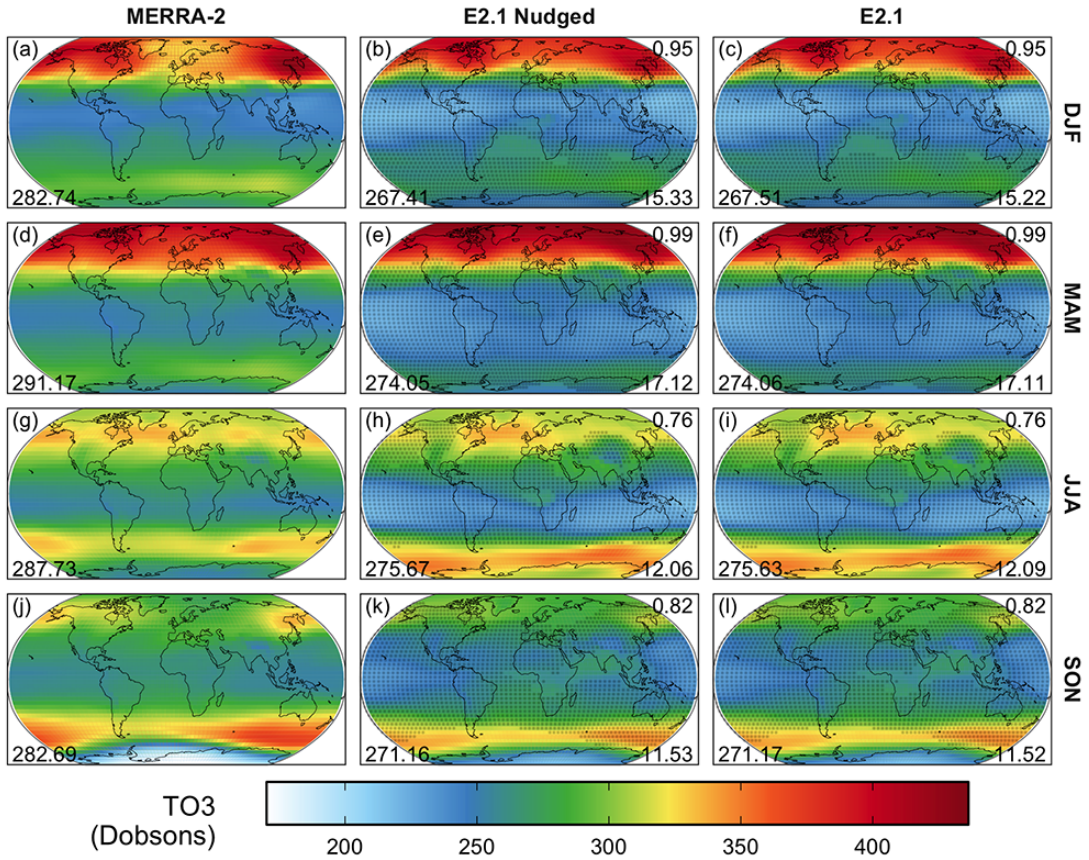


**Figure S22:** The same as Fig. S2, but for total ozone column used in the general circulation model (units: Dobson Units; variable name: TO3).

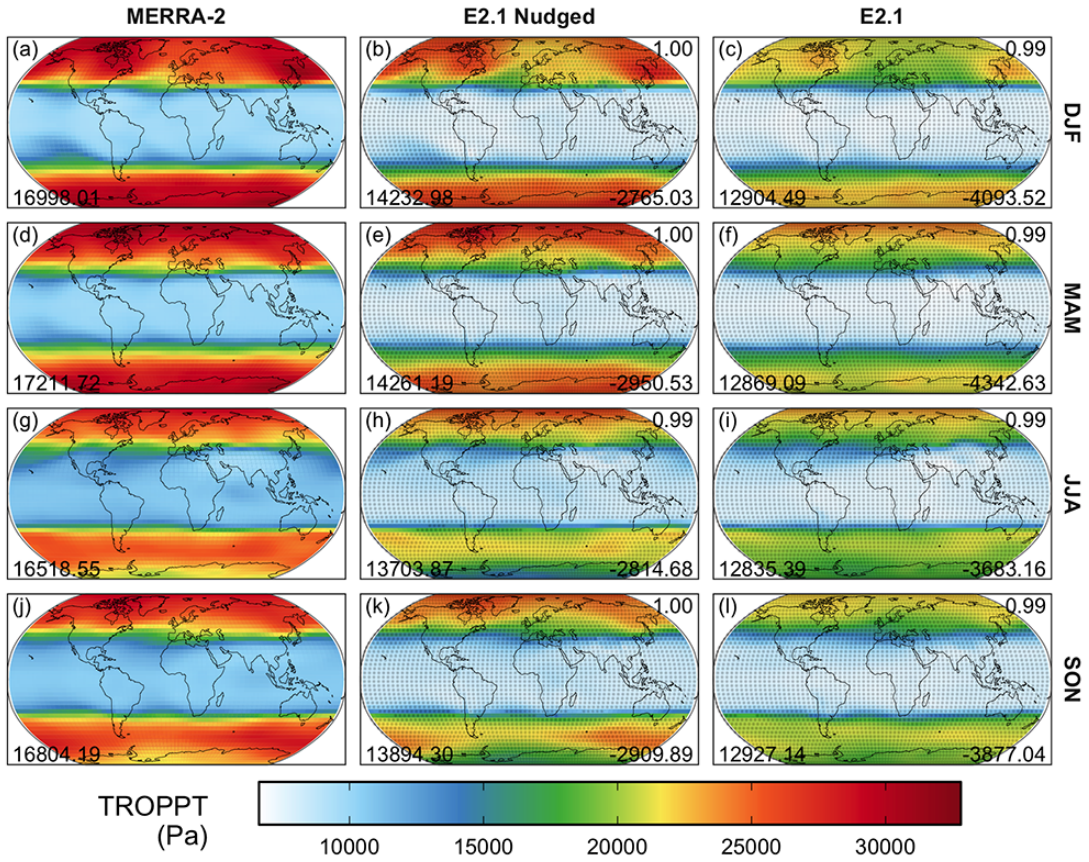


**Figure S23:** The same as Fig. S2, but for tropopause pressure (units: Pa; variable name: TROPPT).

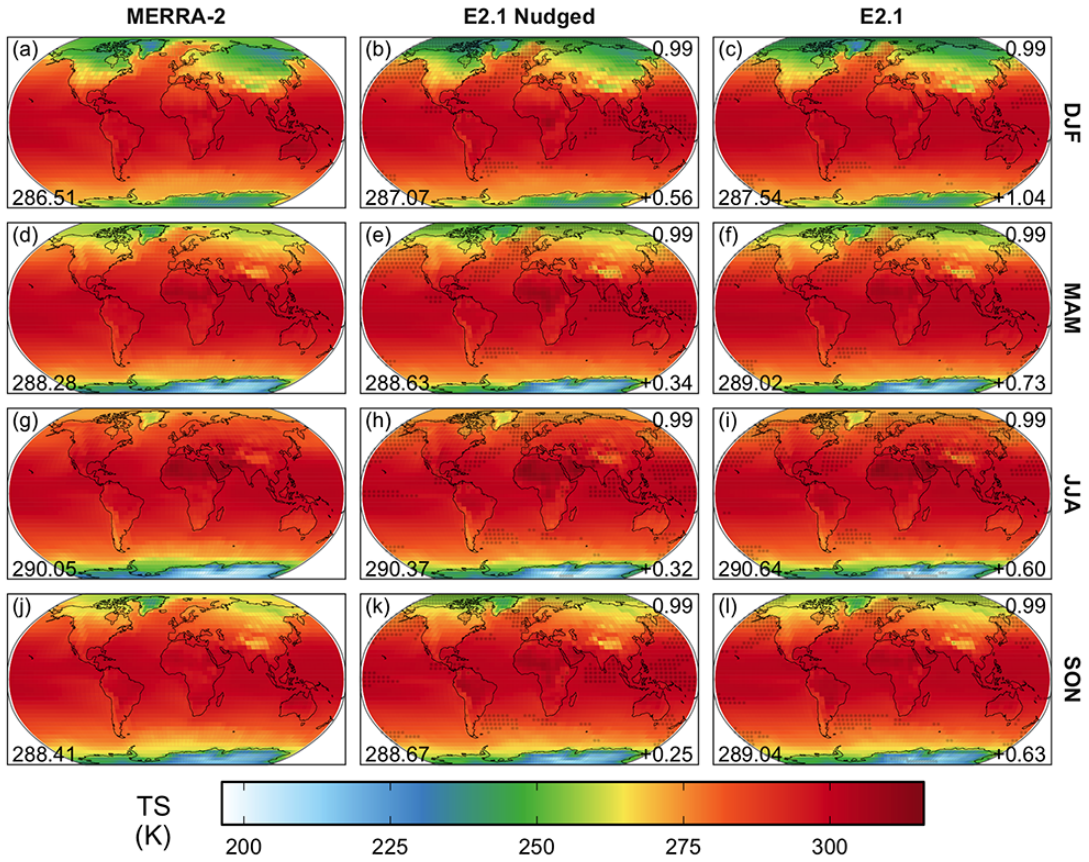


**Figure S24:** The same as Fig. S2, but for the surface skin (land- and sea-surface) temperature (units: K; variable name: TS).



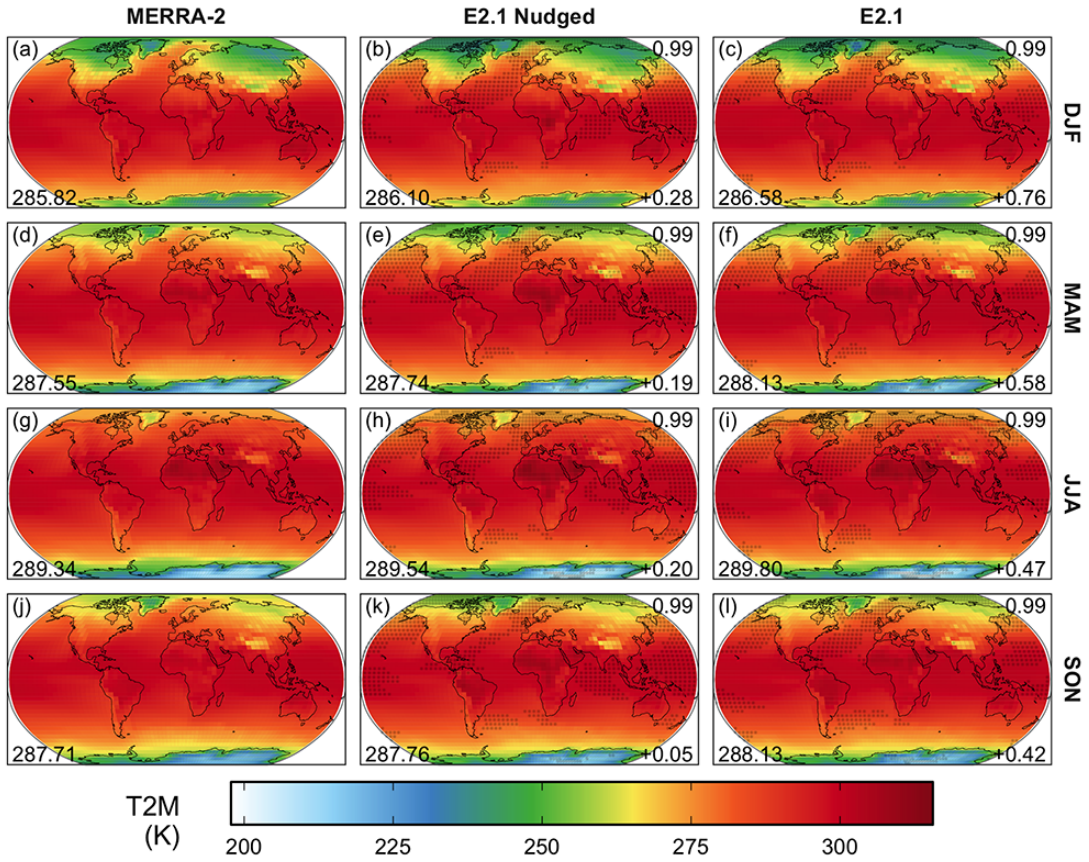


**Figure S25:** The same as Fig. S2, but for the atmospheric temperature at 2 m above the surface (units: K; variable name: T2M).



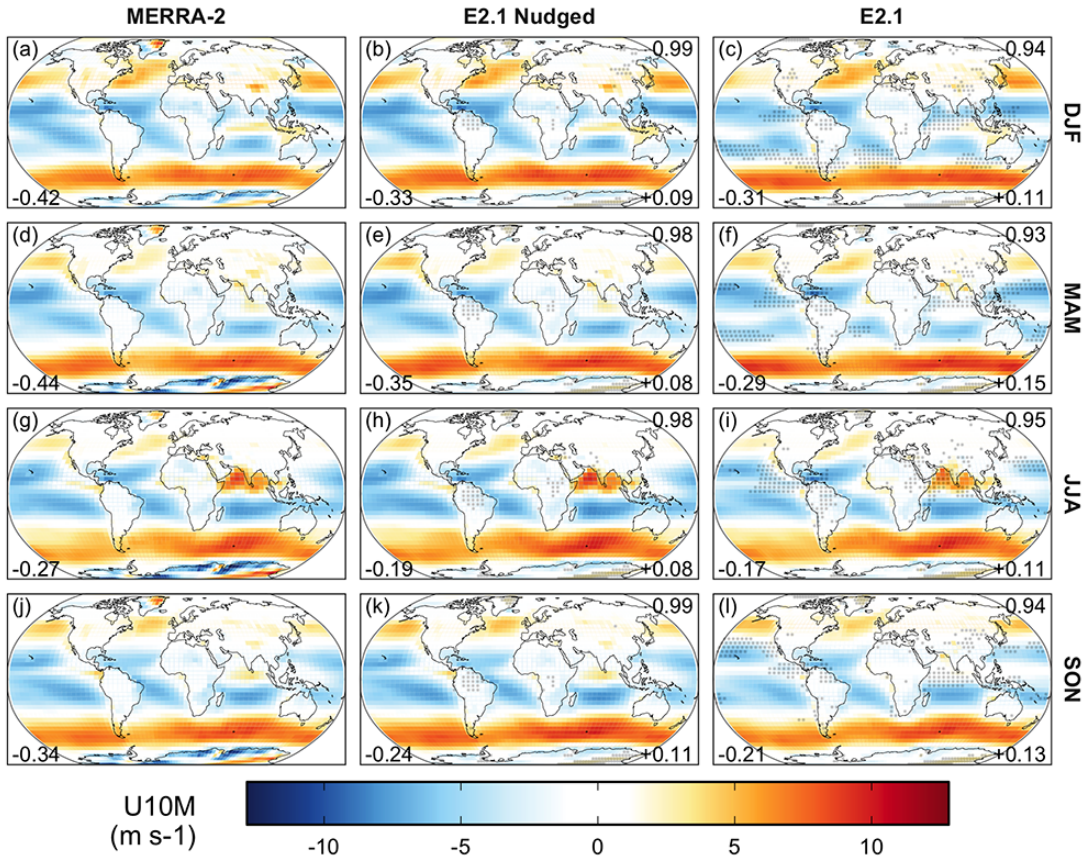


**Figure S26:** The same as Fig. S2, but for the zonal wind component at 10 m above the surface (units: m s<sup>-1</sup>; variable name: U10M).

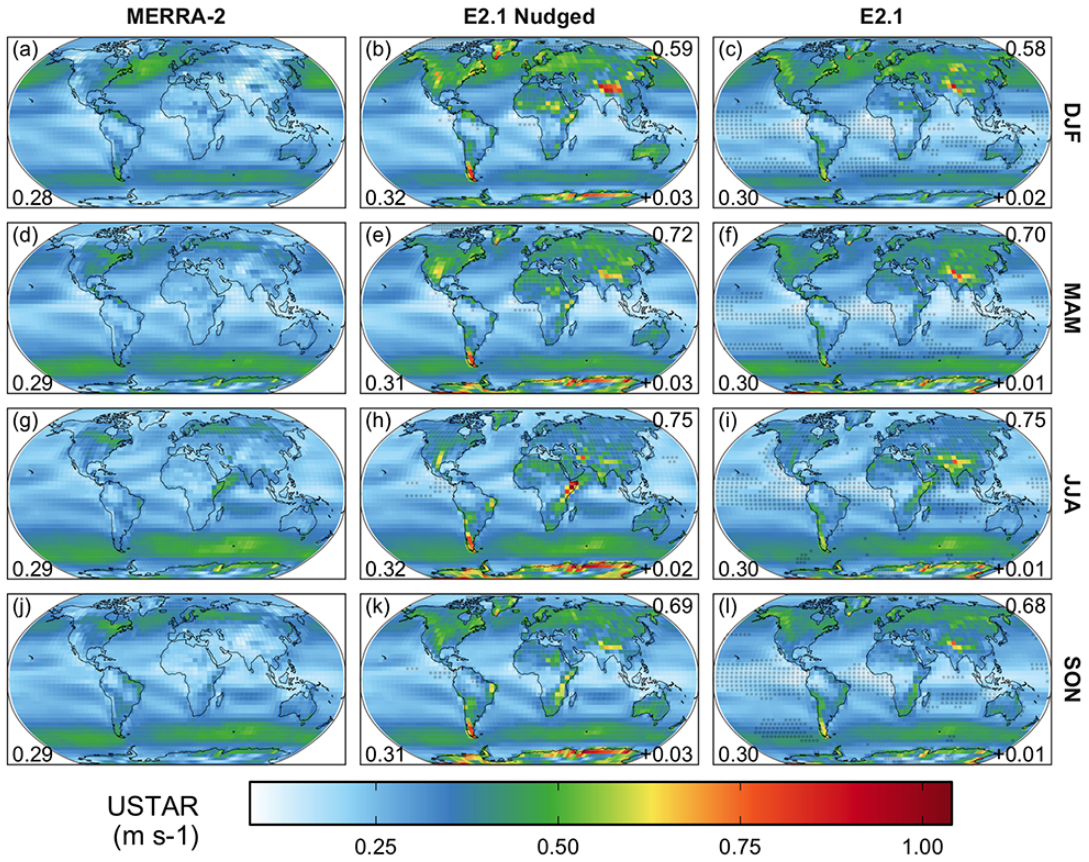


**Figure S27:** The same as Fig. S2, but for the surface friction velocity (units: m s<sup>-1</sup>; variable name: USTAR).

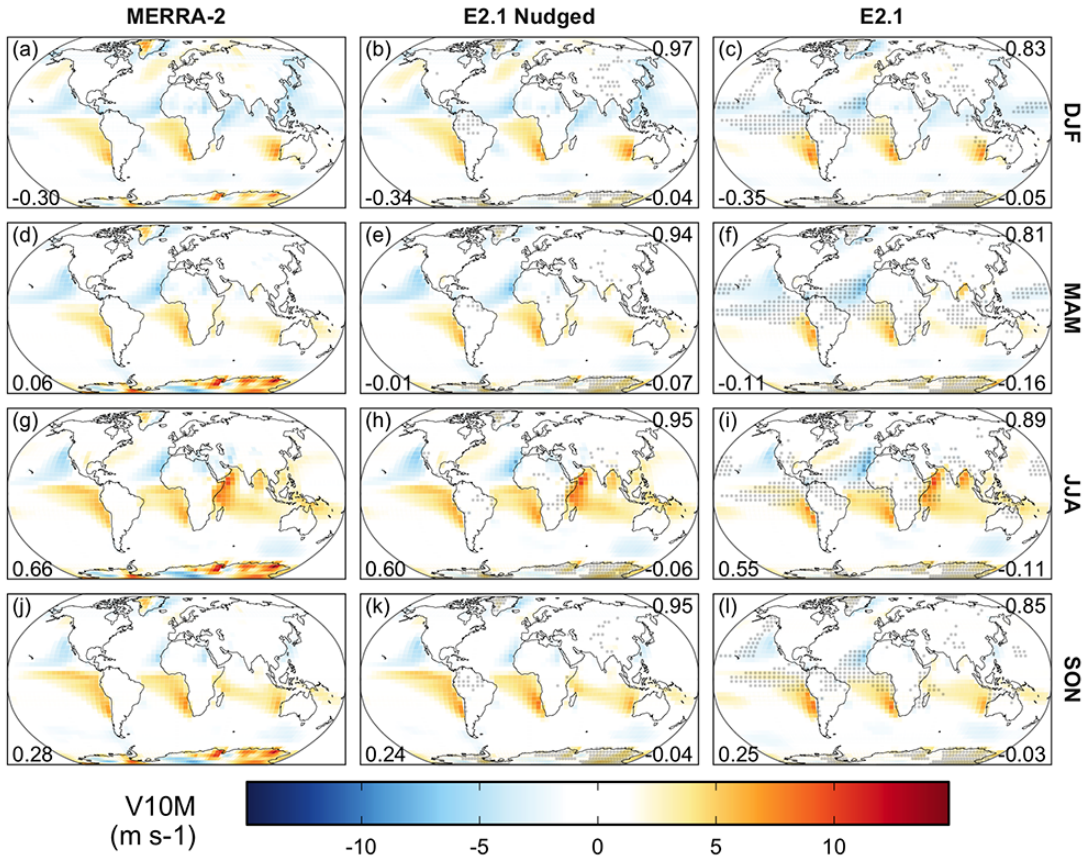


**Figure S28:** The same as Fig. S2, but for the meridional wind component at 10 m above the surface (units: m s<sup>-1</sup>; variable name: V10M).



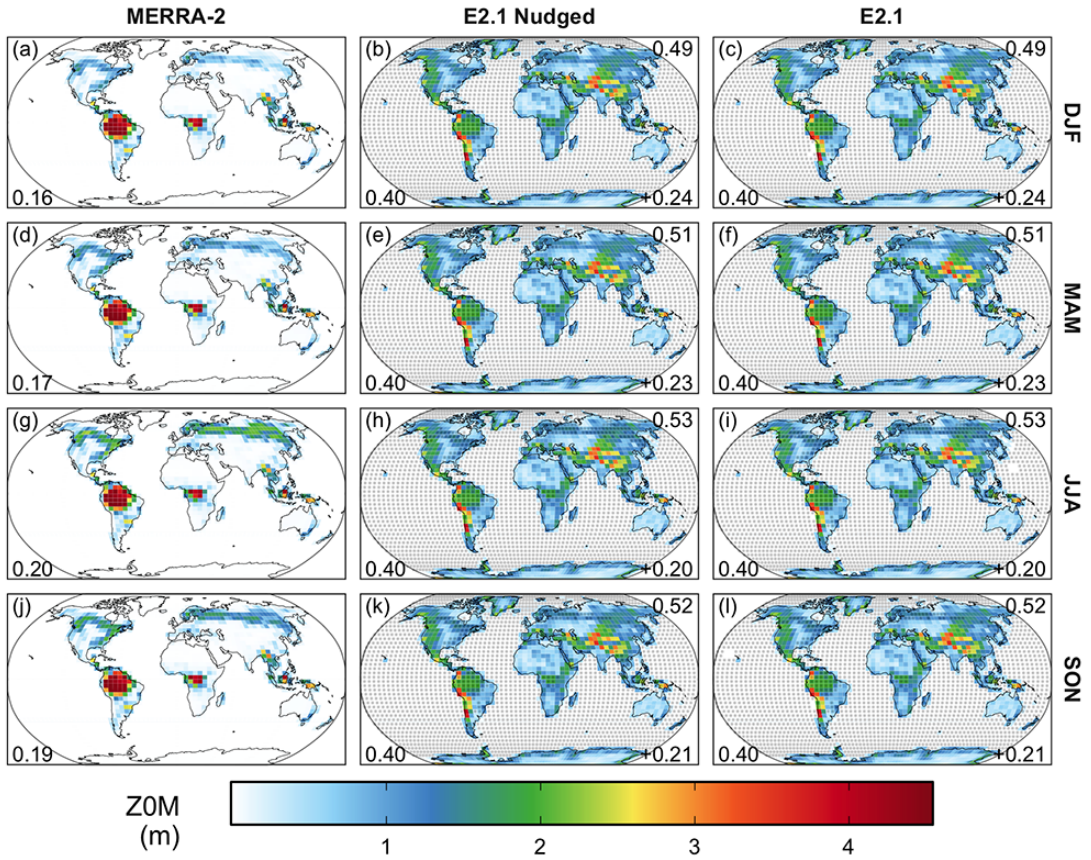


**Figure S29:** The same as Fig. S2, but for surface roughness (units: m; variable name: ZOM).

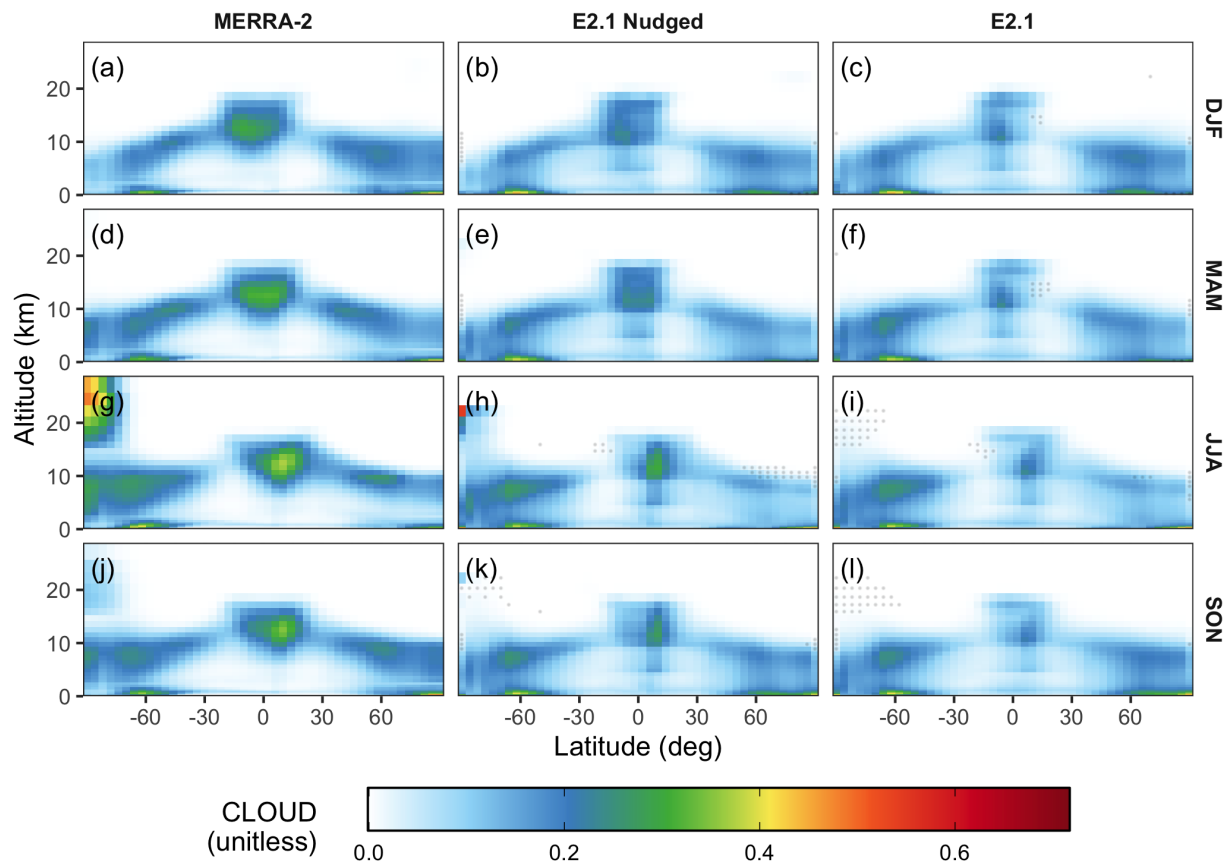


**Figure S30:** Seasonal zonal mean climatology of cloud fraction (unitless; variable name: CLOUD). Rows from top to bottom show the 10-year seasonal average for 2005-2014 C.E. for December-January-February (DJF), March-April-May (MAM), June-July-August (JJA), and September-October-November (SON). Columns from left to right show the values from the MERRA-2 reanalysis (Gelaro et al., 2017), E2.1 nudged to MERRA-2, and the free-running E2.1. Gray dots indicate locations where the E2.1 simulations are statistically different with respect to interannual variability ( $p$ -value  $< 0.05$ ;  $n = 10$  yr).

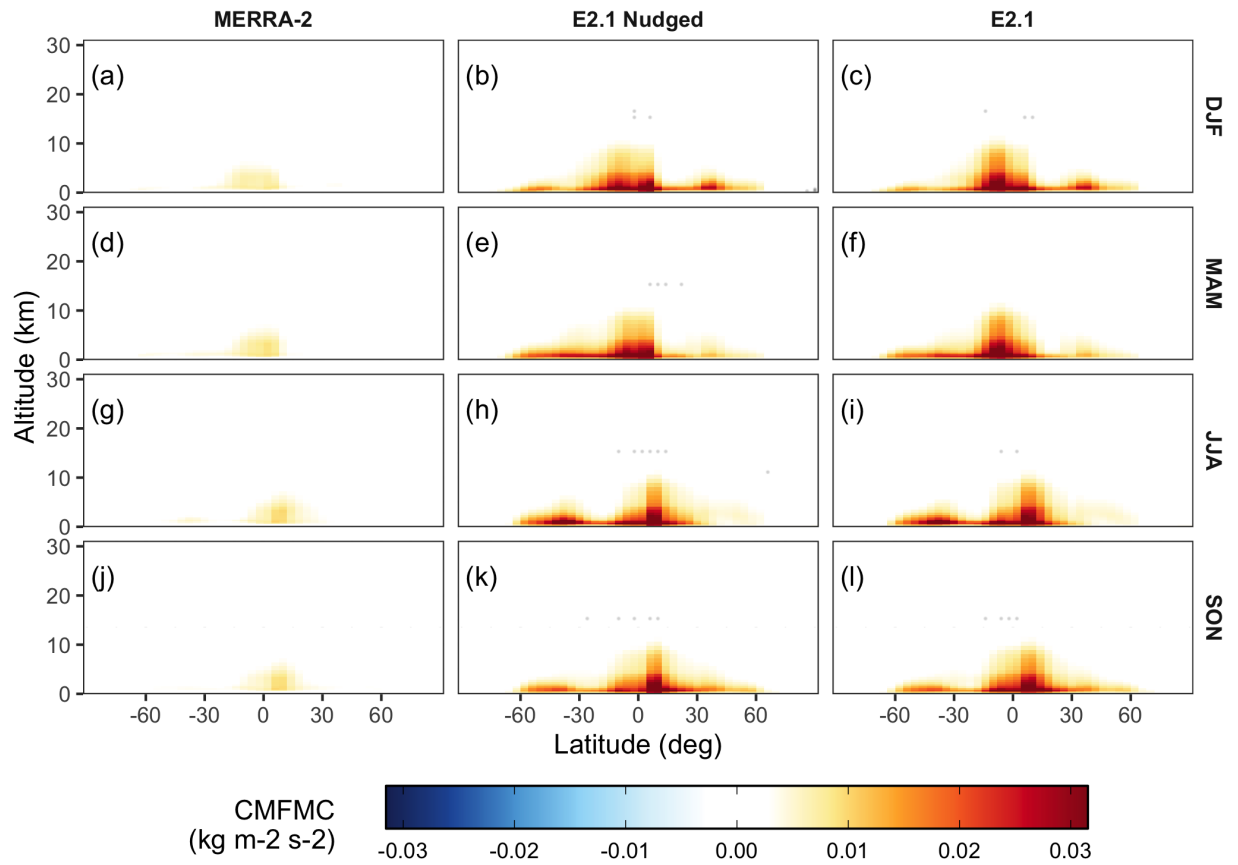


**Figure S31:** The same as Fig. S30, but for the zonal mean upward moist convective mass flux (units:  $\text{kg m}^{-2} \text{s}^{-2}$ ; variable name: CMFMC).

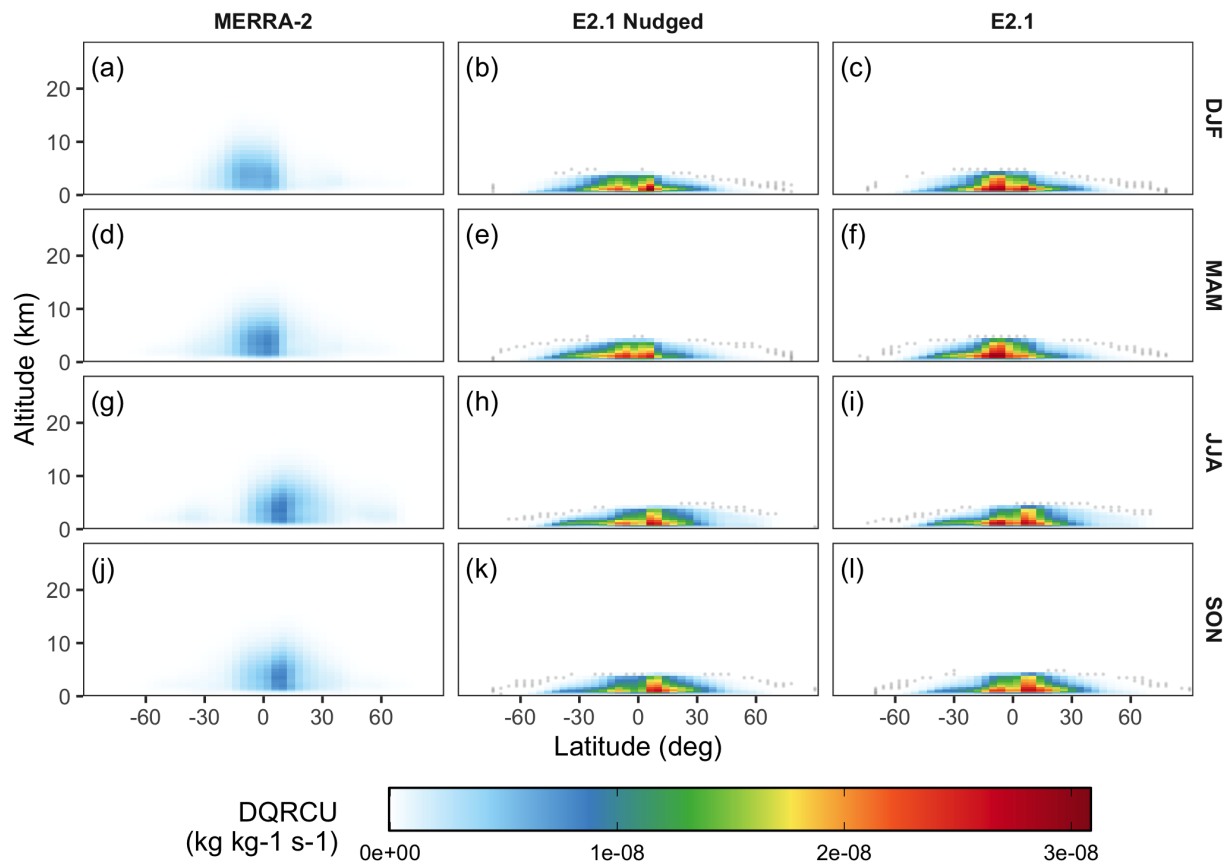


**Figure S32:** The same as Fig. S30, but for the zonal mean convective precipitation source (units:  $\text{kg kg}^{-1} \text{s}^{-1}$ ; variable name: DQRCU).

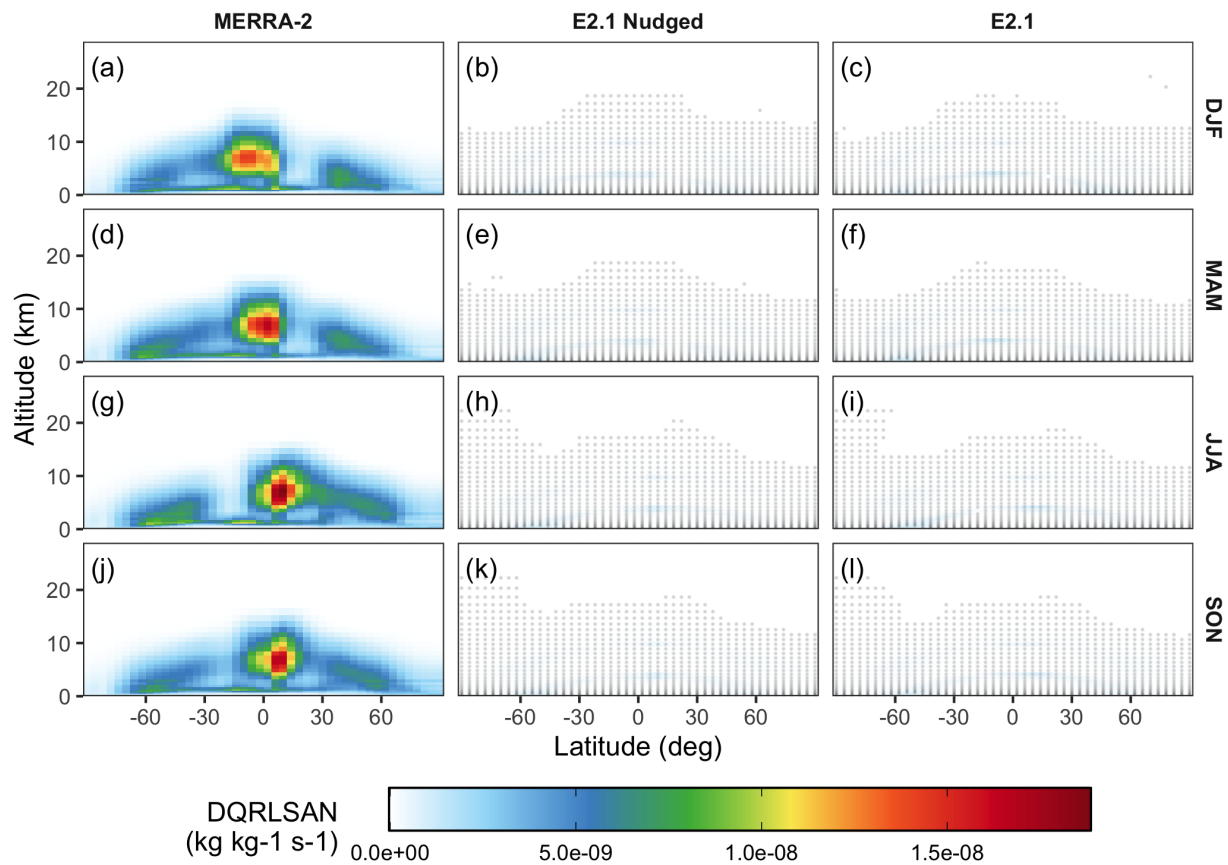


**Figure S33:** The same as Fig. S30, but for the zonal mean stratiform and anvil precipitation source (units:  $\text{kg kg}^{-1} \text{s}^{-1}$ ; variable name: DQRLSAN).



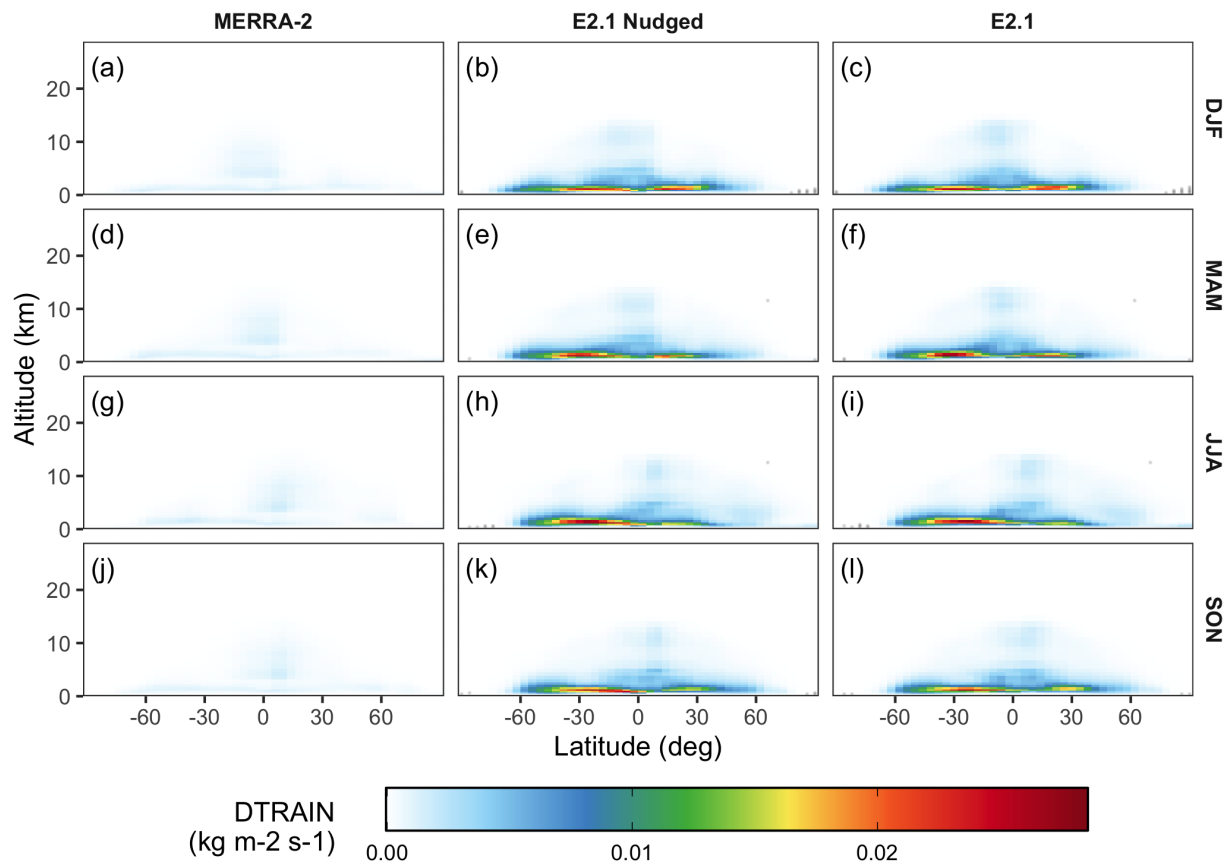


**Figure S34:** The same as Fig. S30, but for the zonal mean detraining mass flux (units:  $\text{kg m}^{-2} \text{s}^{-1}$ ; variable name: DTRAIN).

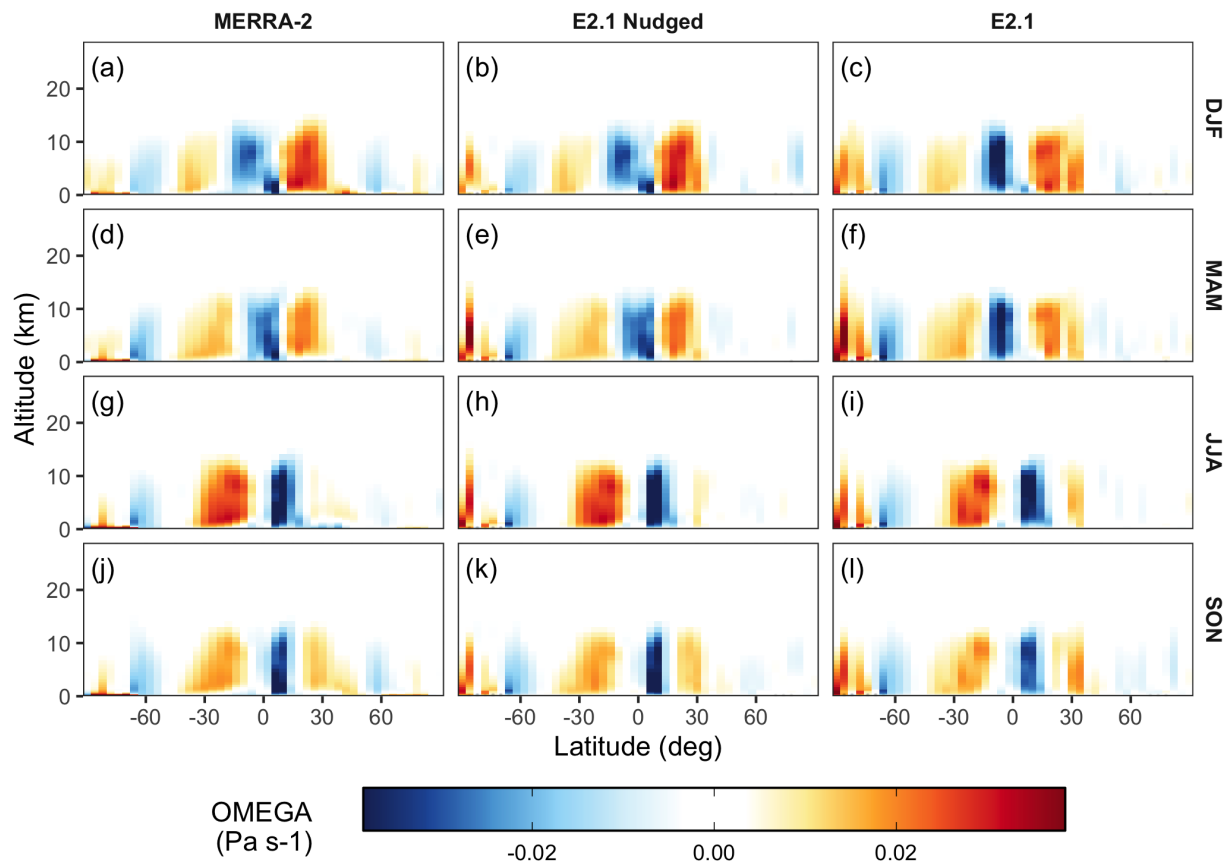


**Figure S35:** The same as Fig. S30, but for the zonal mean vertical pressure velocity (units:  $\text{Pa s}^{-1}$ ; variable name: OMEGA).

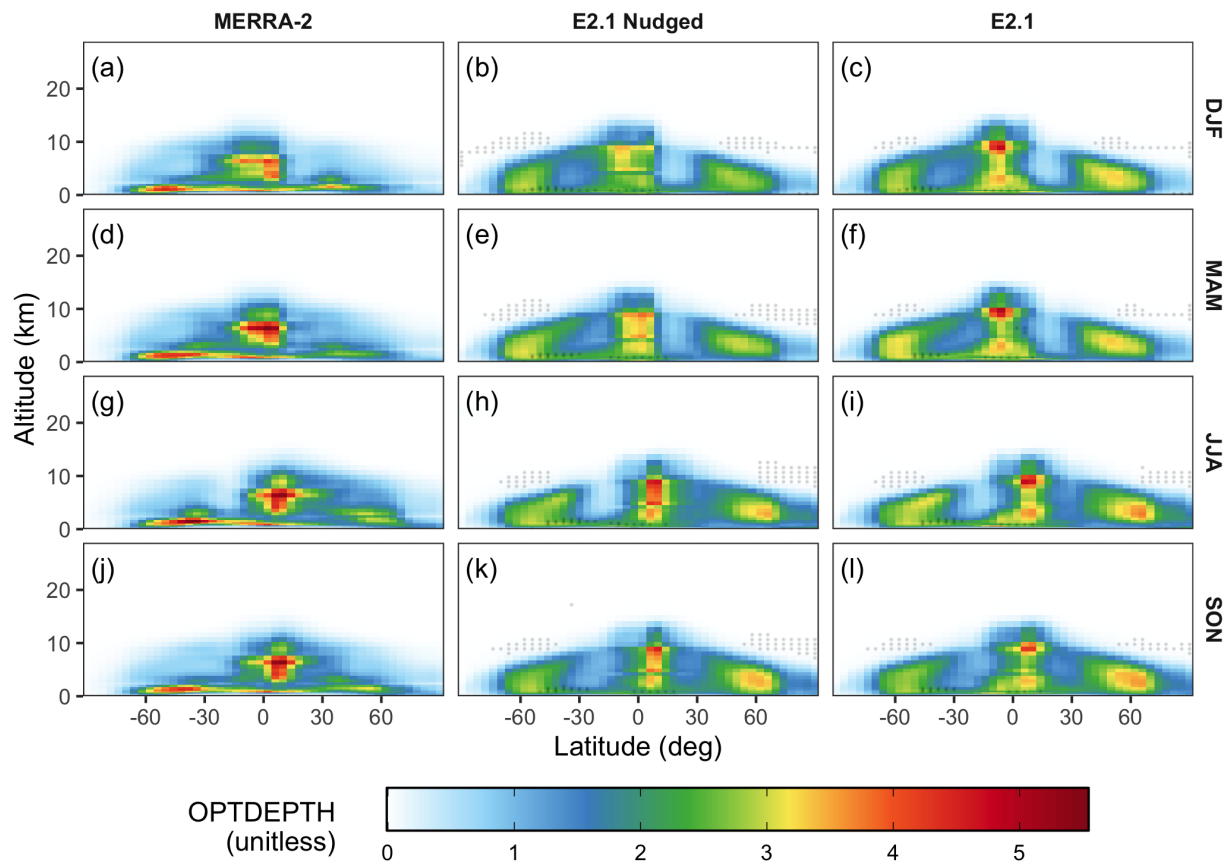


**Figure S36:** The same as Fig. S30, but for the zonal mean in-cloud optical depth (unitless; variable name: OPTDEPTH).

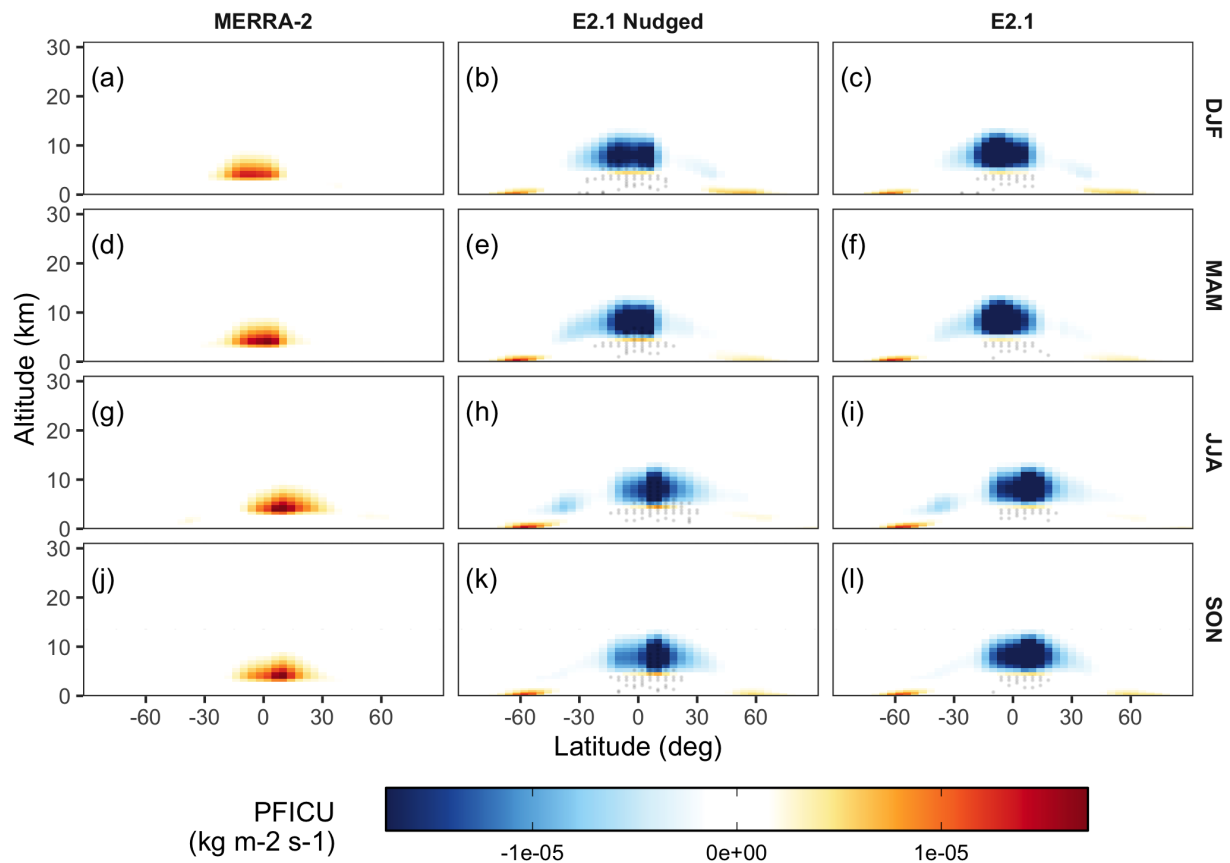


**Figure S37:** The same as Fig. S30, but for the zonal mean flux of ice precipitation from convection (units:  $\text{kg m}^{-2} \text{s}^{-1}$ ; variable name: PFICU).



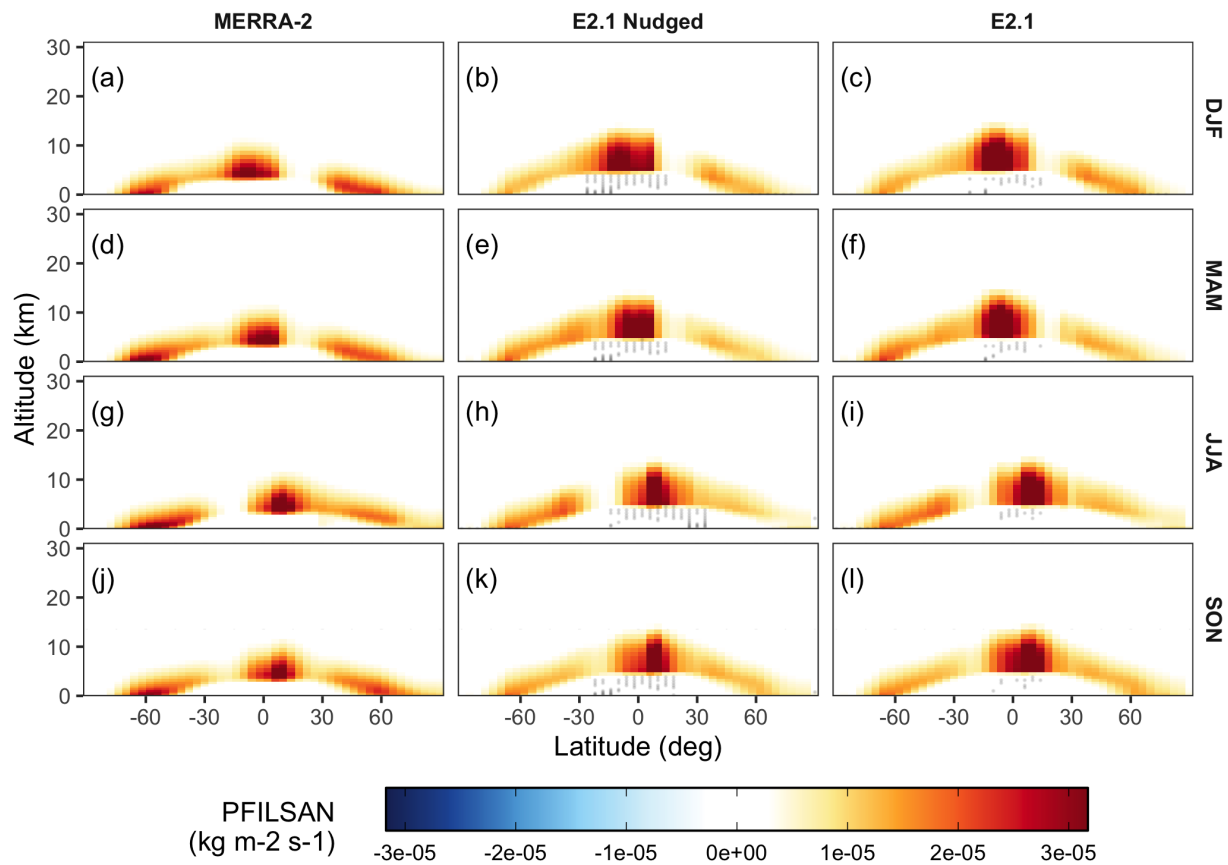


**Figure S38:** The same as Fig. S30, but for the zonal mean flux of ice precipitation from stratiform clouds (units:  $\text{kg m}^{-2} \text{s}^{-1}$ ; variable name: PFILSAN).

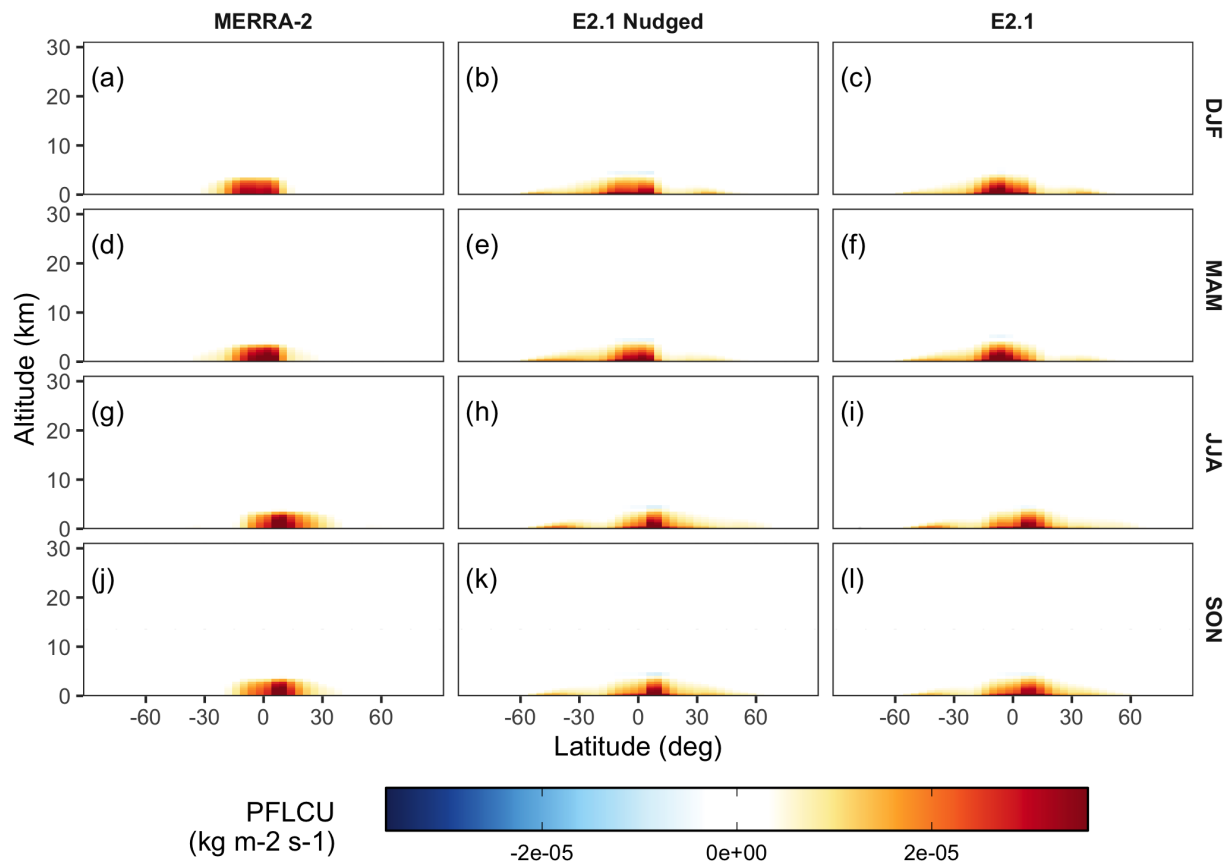


**Figure S39:** The same as Fig. S30, but for the zonal mean flux of liquid precipitation from convection (units:  $\text{kg m}^{-2} \text{s}^{-1}$ ; variable name: PFLCU).

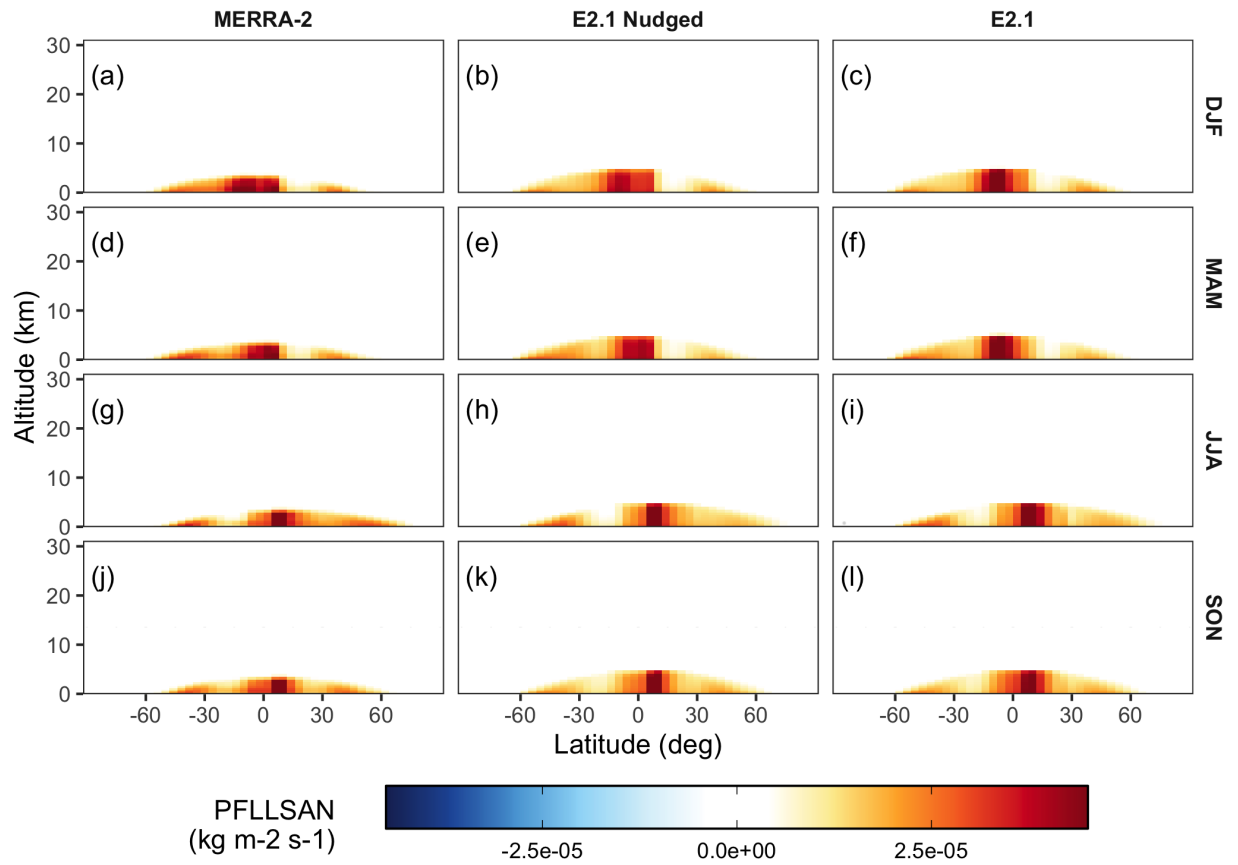


**Figure S40:** The same as Fig. S30, but for the zonal mean flux of liquid precipitation from stratiform clouds (units:  $\text{kg m}^{-2} \text{s}^{-1}$ ; variable name: PFLLSAN).

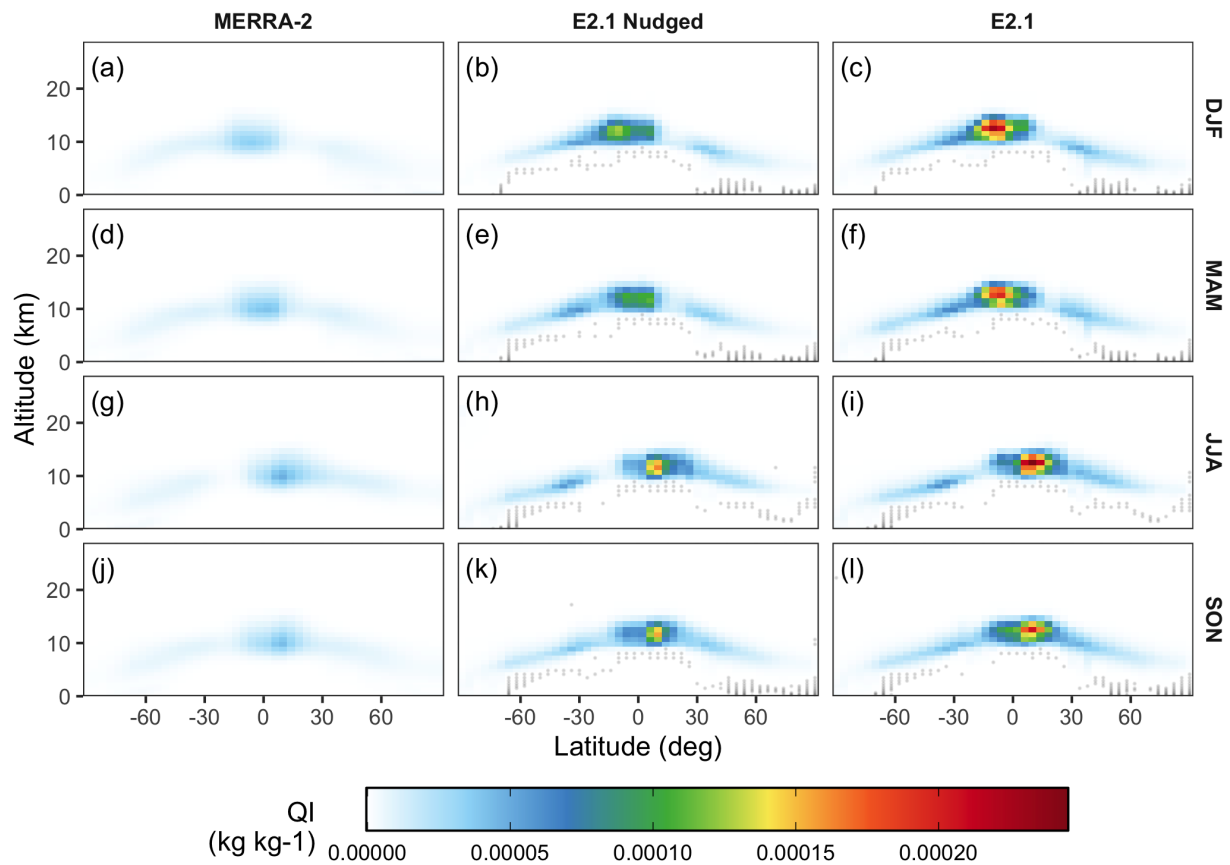


**Figure S41:** The same as Fig. S30, but for the zonal mean mass fraction of cloud ice water (units:  $\text{kg kg}^{-1}$ ; variable name: QI).



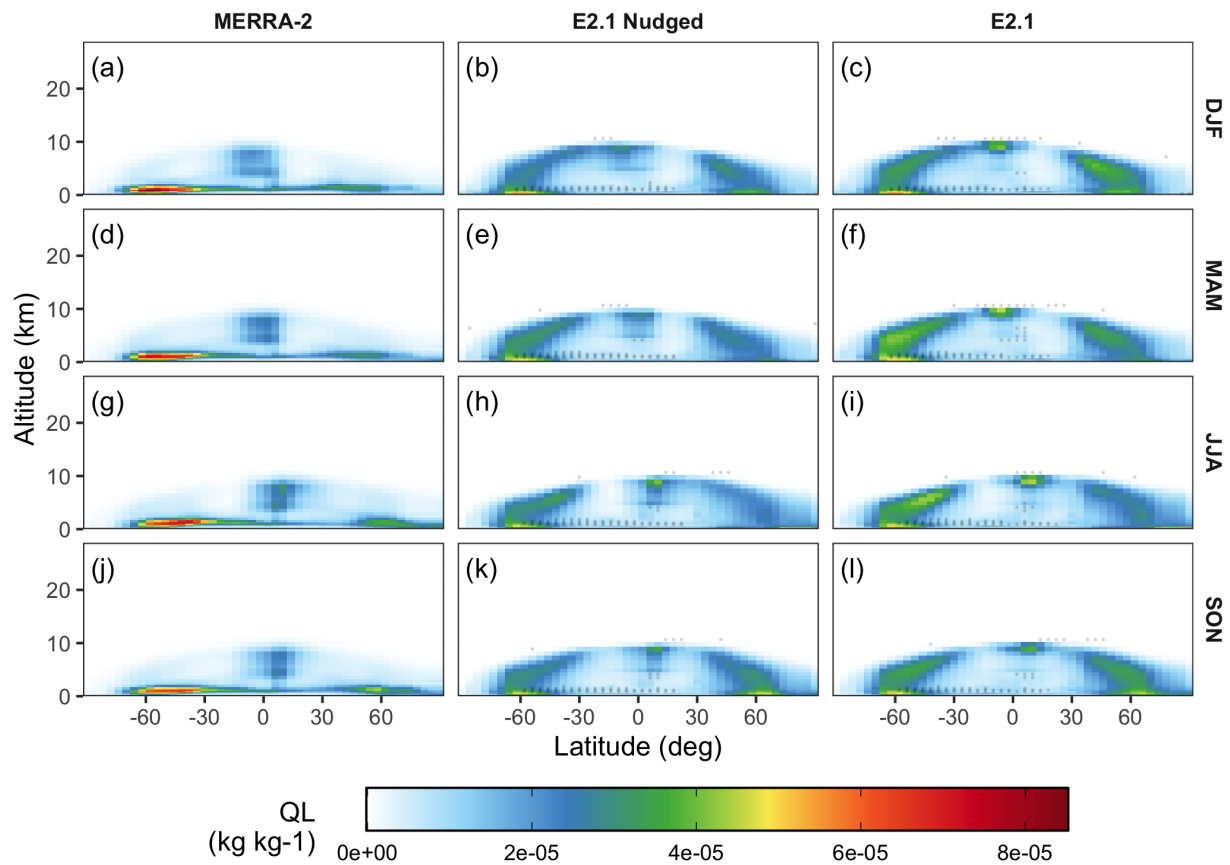


**Figure S42:** The same as Fig. S30, but for the zonal mean mass fraction of cloud liquid water (units:  $\text{kg kg}^{-1}$ ; variable name: QL).

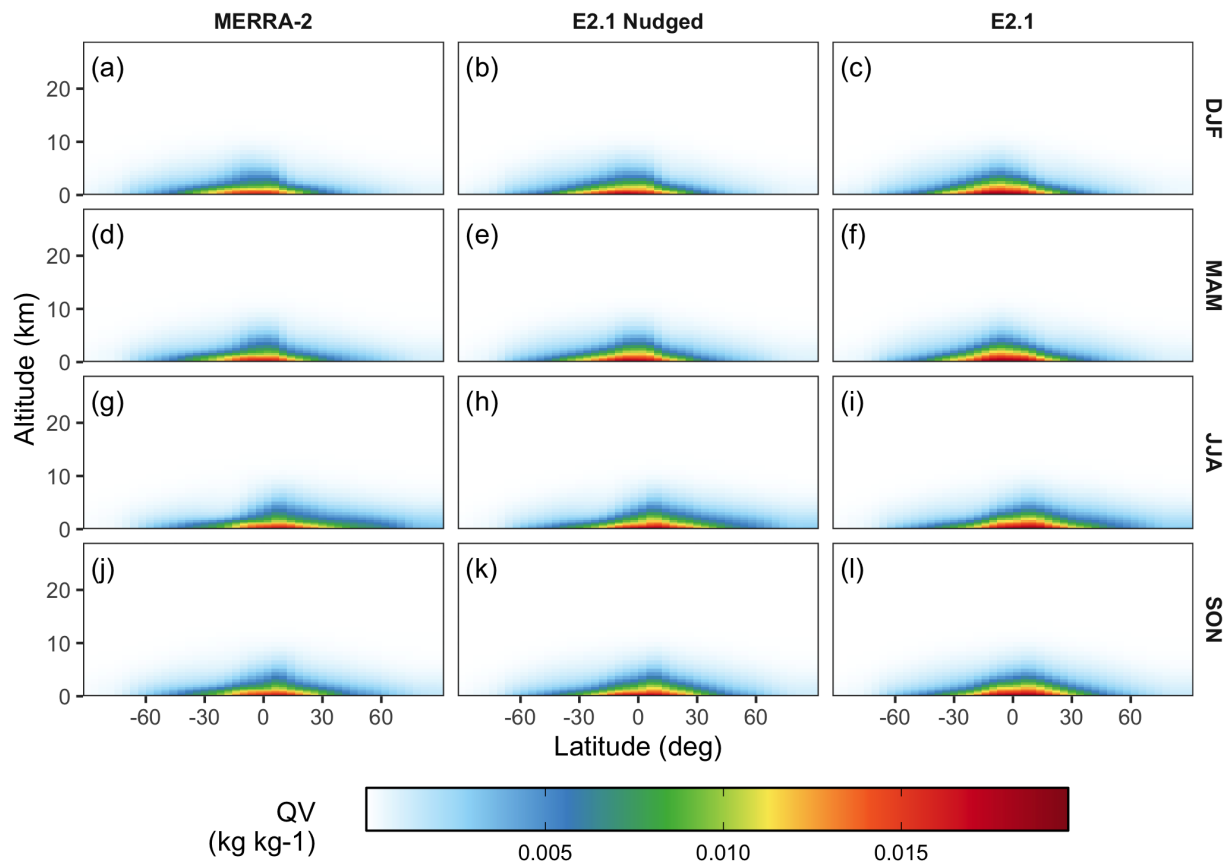


**Figure S43:** The same as Fig. S30, but for the zonal mean specific humidity (units:  $\text{kg kg}^{-1}$ ; variable name: QV).

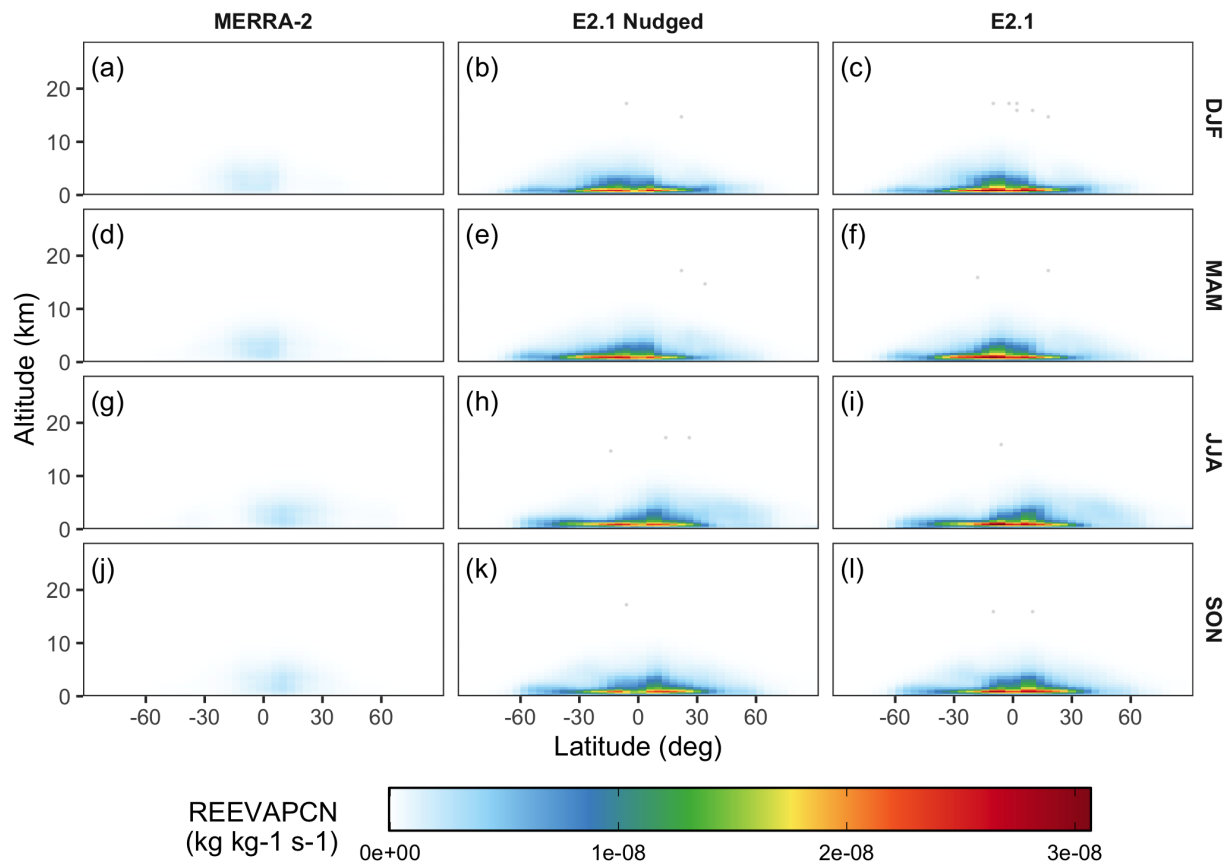


**Figure S44:** The same as Fig. S30, but for the zonal mean evaporation and sublimation of convective precipitation (units:  $\text{kg kg}^{-1} \text{s}^{-1}$ ; variable name: REEVAPCN).

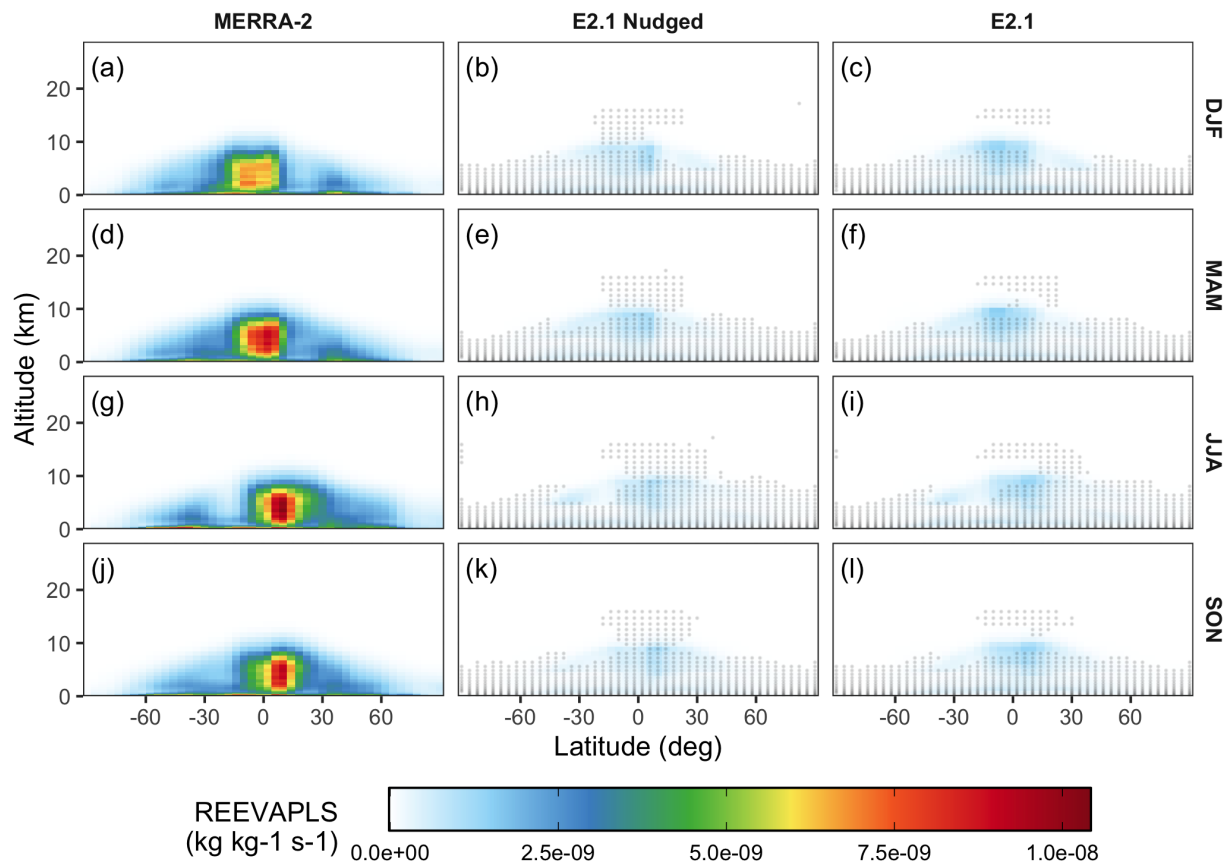


**Figure S45:** The same as Fig. S30, but for the zonal mean evaporation and sublimation of stratiform and anvil precipitation (units:  $\text{kg kg}^{-1} \text{s}^{-1}$ ; variable name: REEVAPLS).



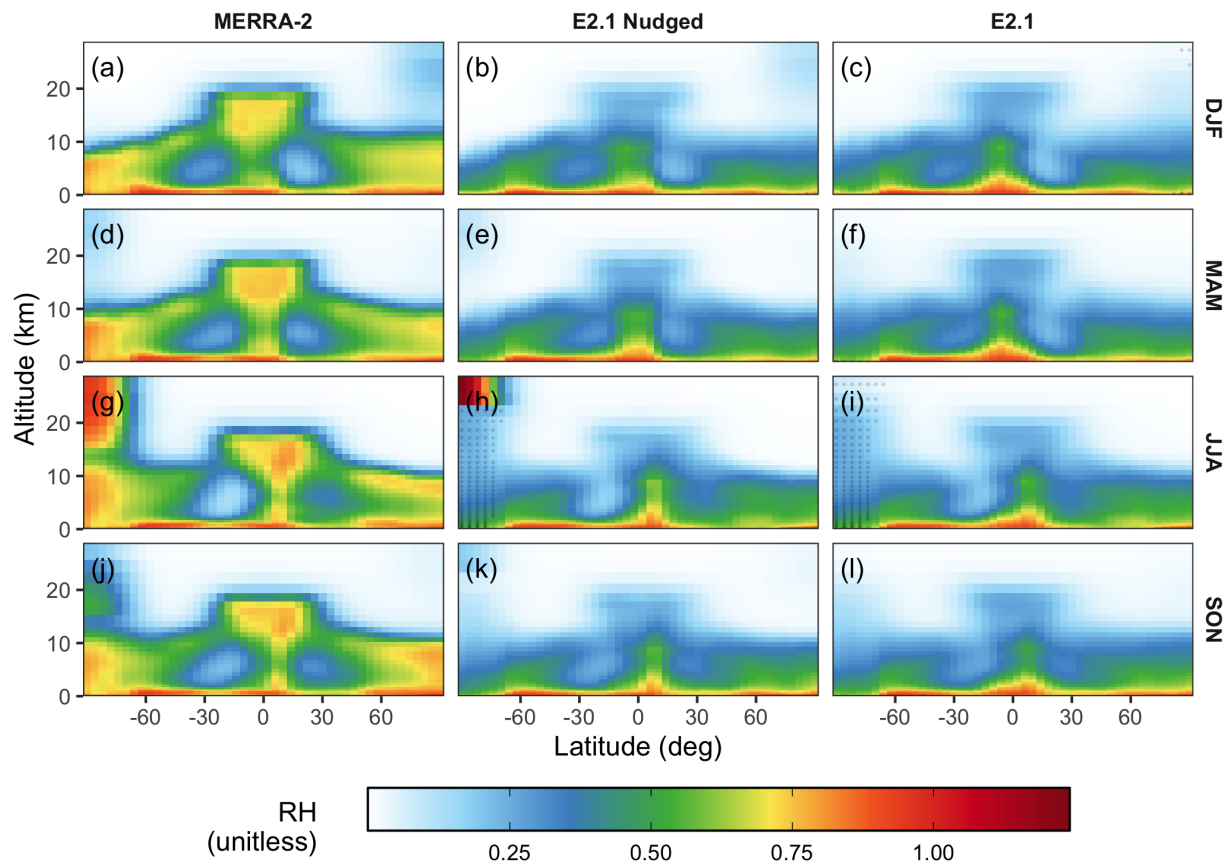


**Figure S46:** The same as Fig. S30, but for the zonal mean relative humidity (unitless; variable name: RH).

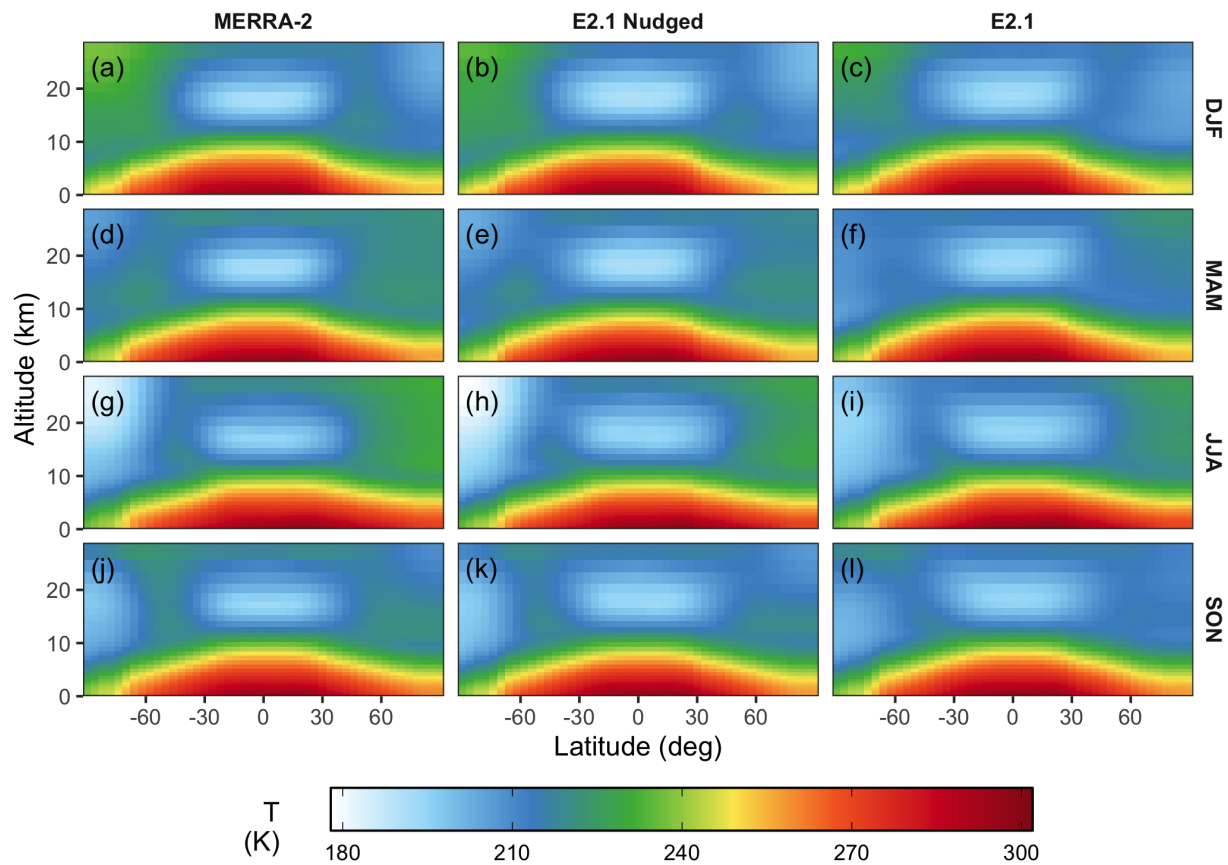


**Figure S47:** The same as Fig. S30, but for the zonal mean temperature (units: K; variable name: T).

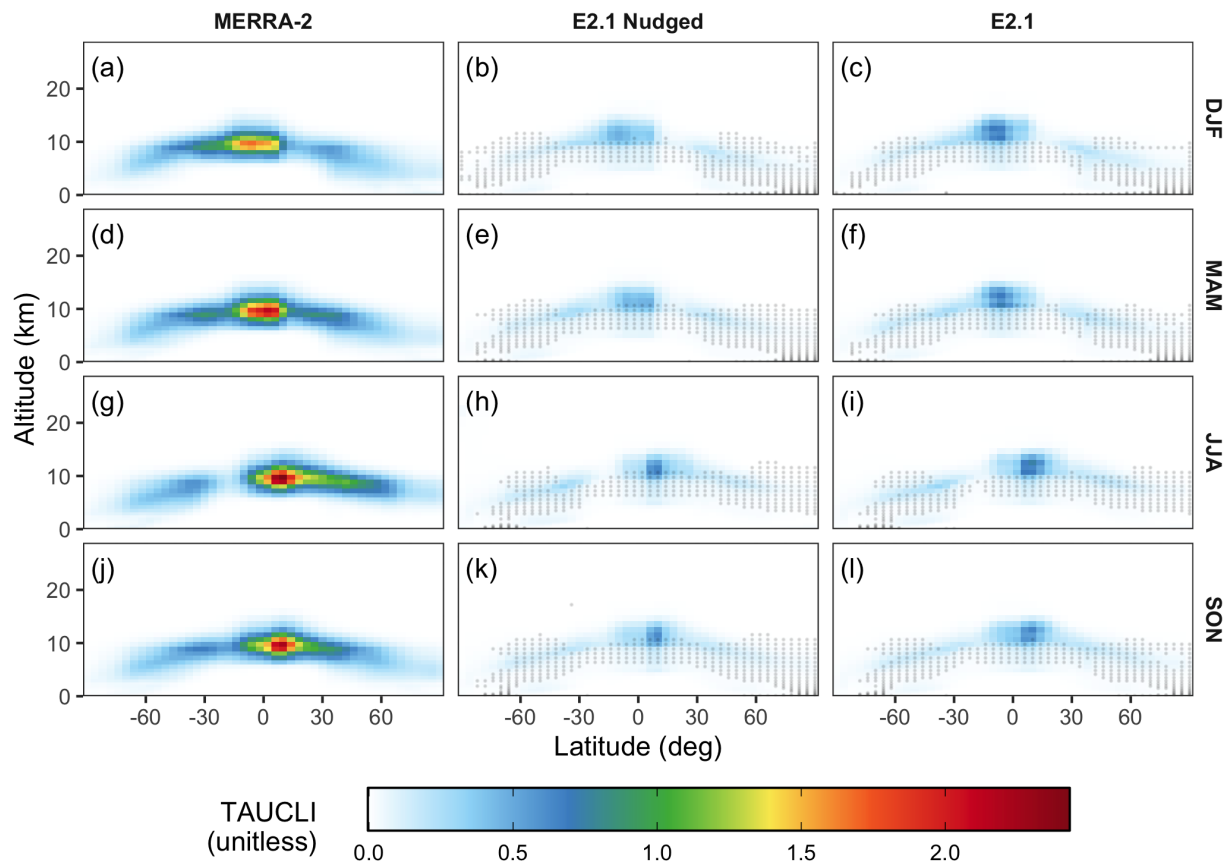


**Figure S48:** The same as Fig. S30, but for the zonal mean in-cloud optical thickness of ice clouds (unitless; variable name: TAUCLI).

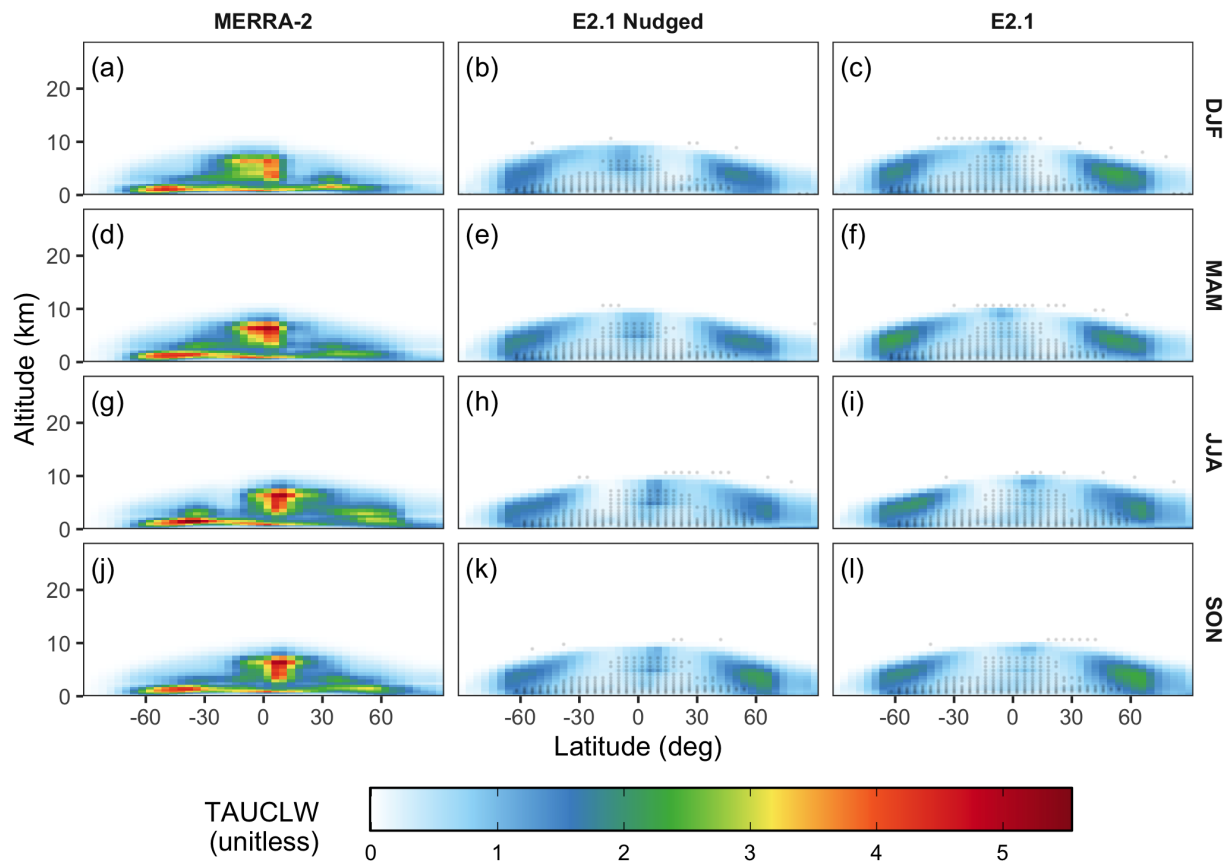


**Figure S49:** The same as Fig. S30, but for the zonal mean in-cloud optical thickness of liquid clouds (unitless; variable name: TAUCLW).



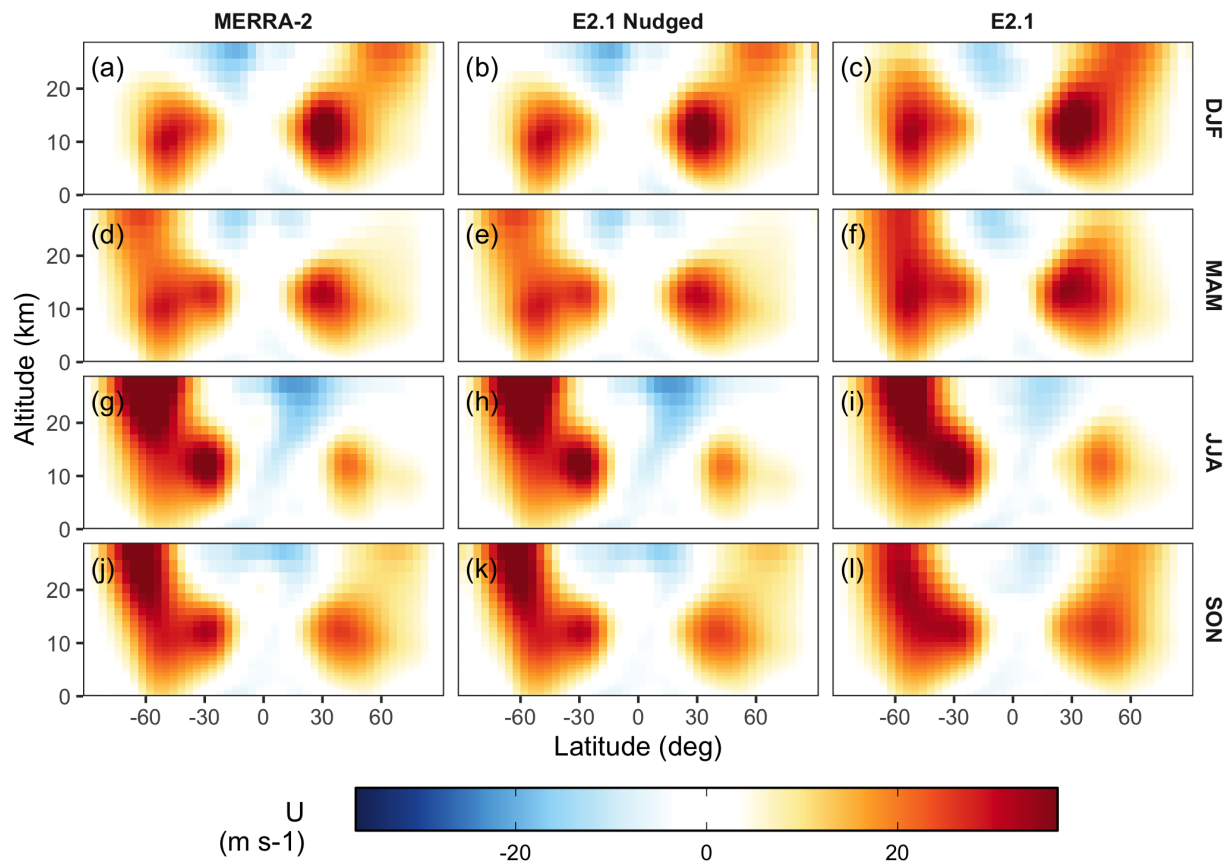


**Figure S50:** The same as Fig. S30, but for the zonal mean zonal wind component (units:  $\text{m s}^{-1}$ ; variable name: U).

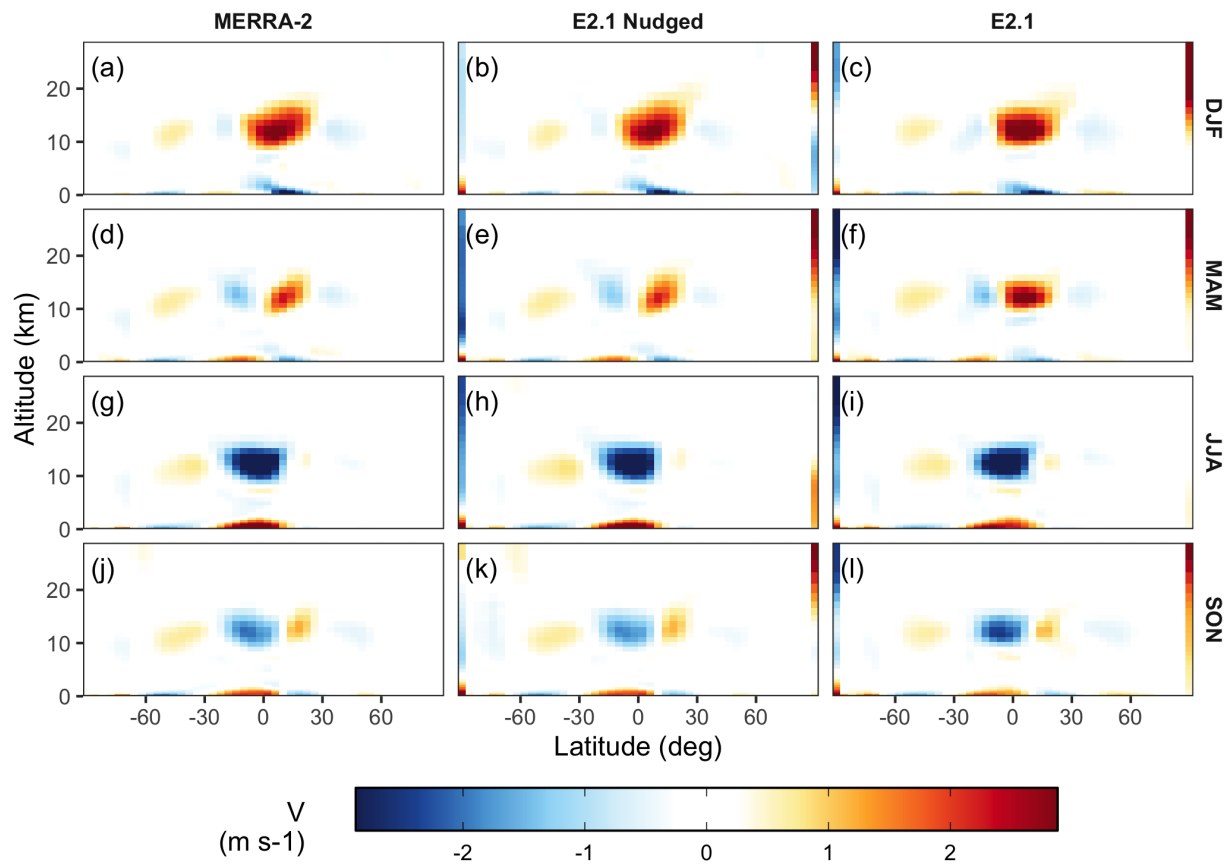


**Figure S51:** The same as Fig. S30, but for the zonal mean meridional wind component (units:  $\text{m s}^{-1}$ ; variable name: V).

## **S2 Emissions**

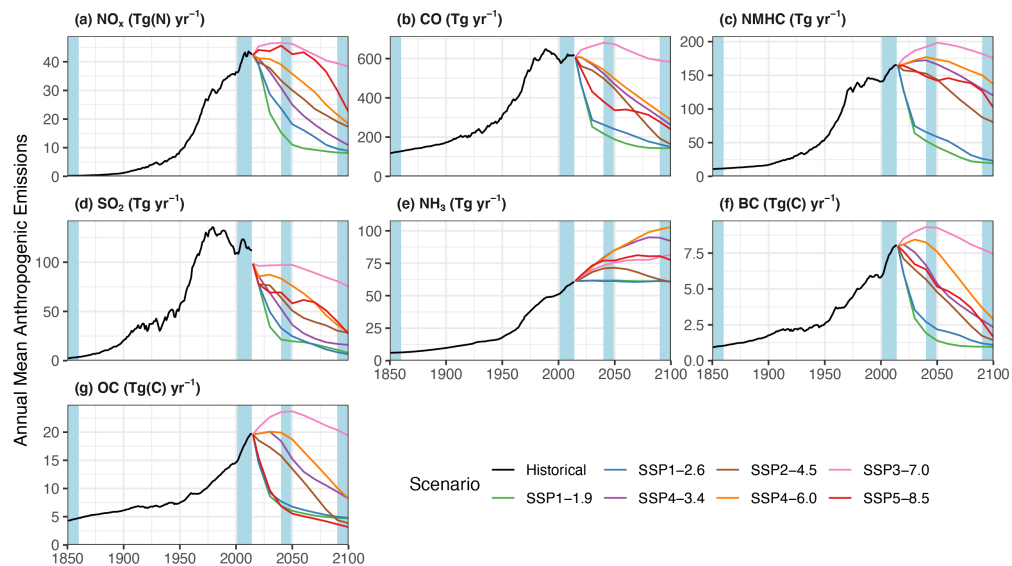


**Figure S52:** The same as Fig. 6 in the main text, but isolating surface anthropogenic emissions excluding open fires.

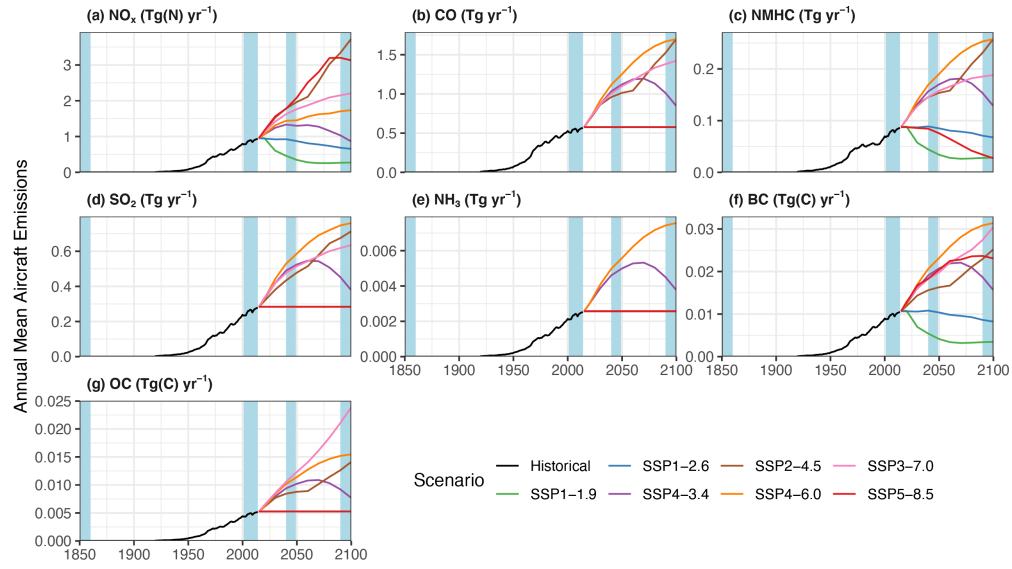


**Figure S53:** The same as Fig. S52, but isolating aircraft emissions.



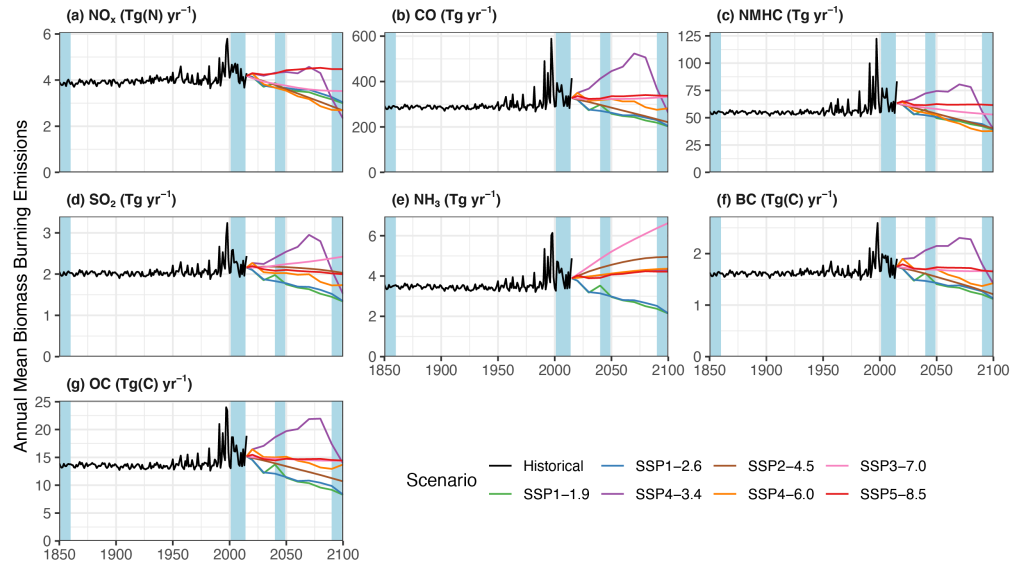


**Figure S54:** The same as Fig. S52, but isolating open fire emissions. Historical emissions are from van Marle et al. (2017) and future emissions from Gidden et al. (2019).

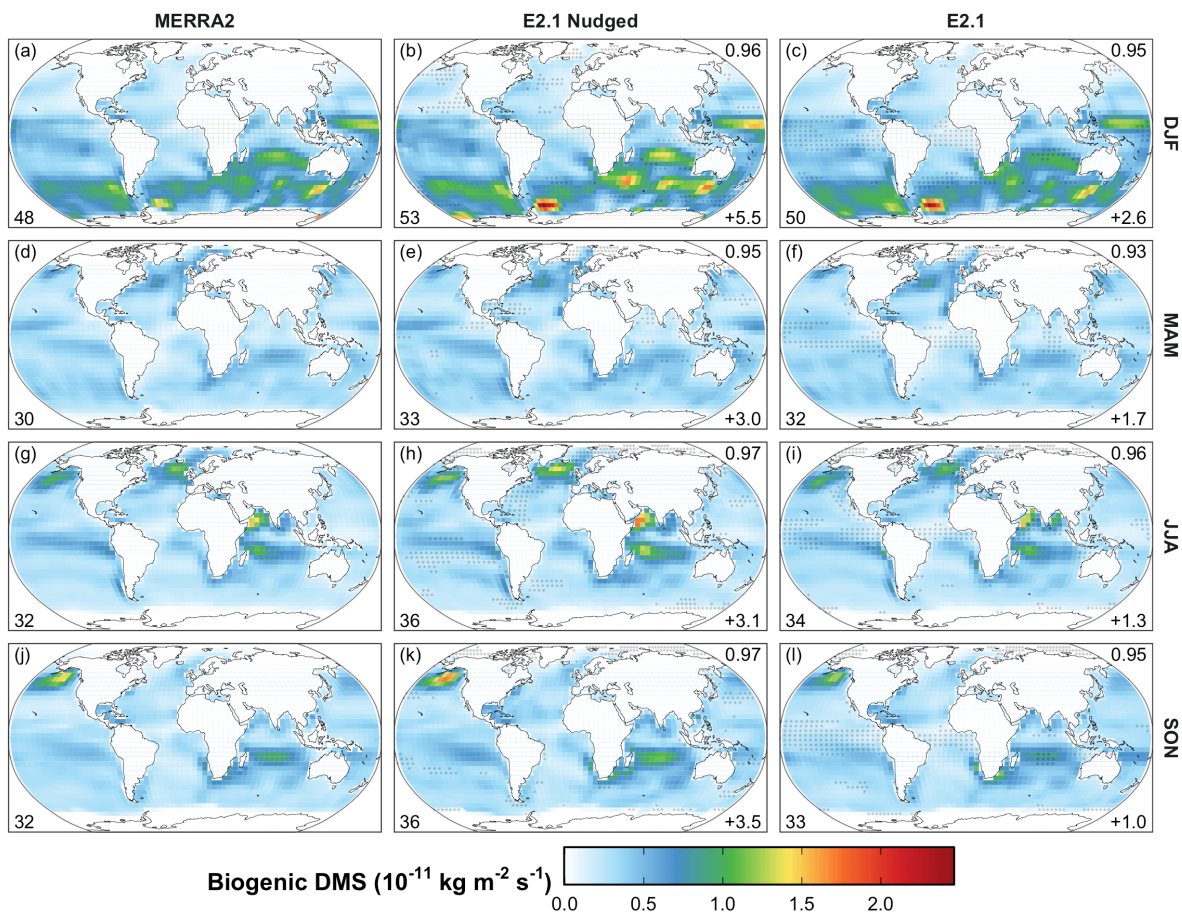


**Figure S55:** Seasonal mean spatial distribution of dimethylsulfide ((CH<sub>3</sub>)<sub>2</sub>S; DMS) emissions from marine biogenic activity for 2005-2014 C.E. Each column from left to right shows emission fluxes calculated using: MERRA-2 meteorology, E2.1 meteorology nudged to MERRA-2, and the free-running E2.1 meteorology, respectively. Each row from top to bottom shows mean emission fluxes for December-January-February (DJF), March-April-May (MAM), June-July-August (JJA), and September-October-November (SON). Gray dots indicate locations where the E2.1-driven simulations show statistically significant differences ( $p$ -value < 0.05;  $n$  = 10 seasons) with respect to the MERRA-2-driven simulation. The value in the lower left of each panel gives the globally integrated source in Tg a<sup>-1</sup>. The number in the lower (upper) right of each panel gives the total difference (pattern correlation) of the E2.1-driven simulations with respect to their respective MERRA-2-driven values.

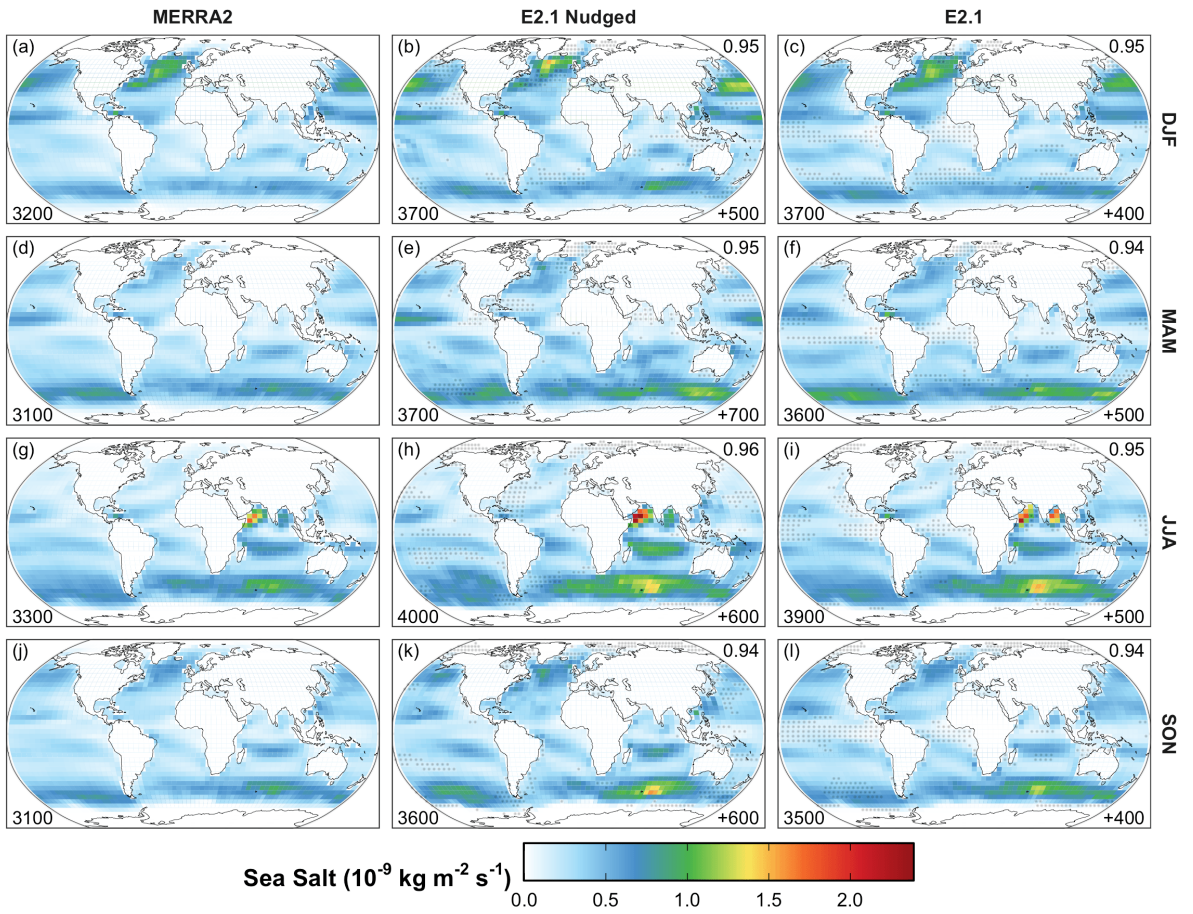


Figure S56: Same as Fig. S55, but for aeolian sea salt emissions.

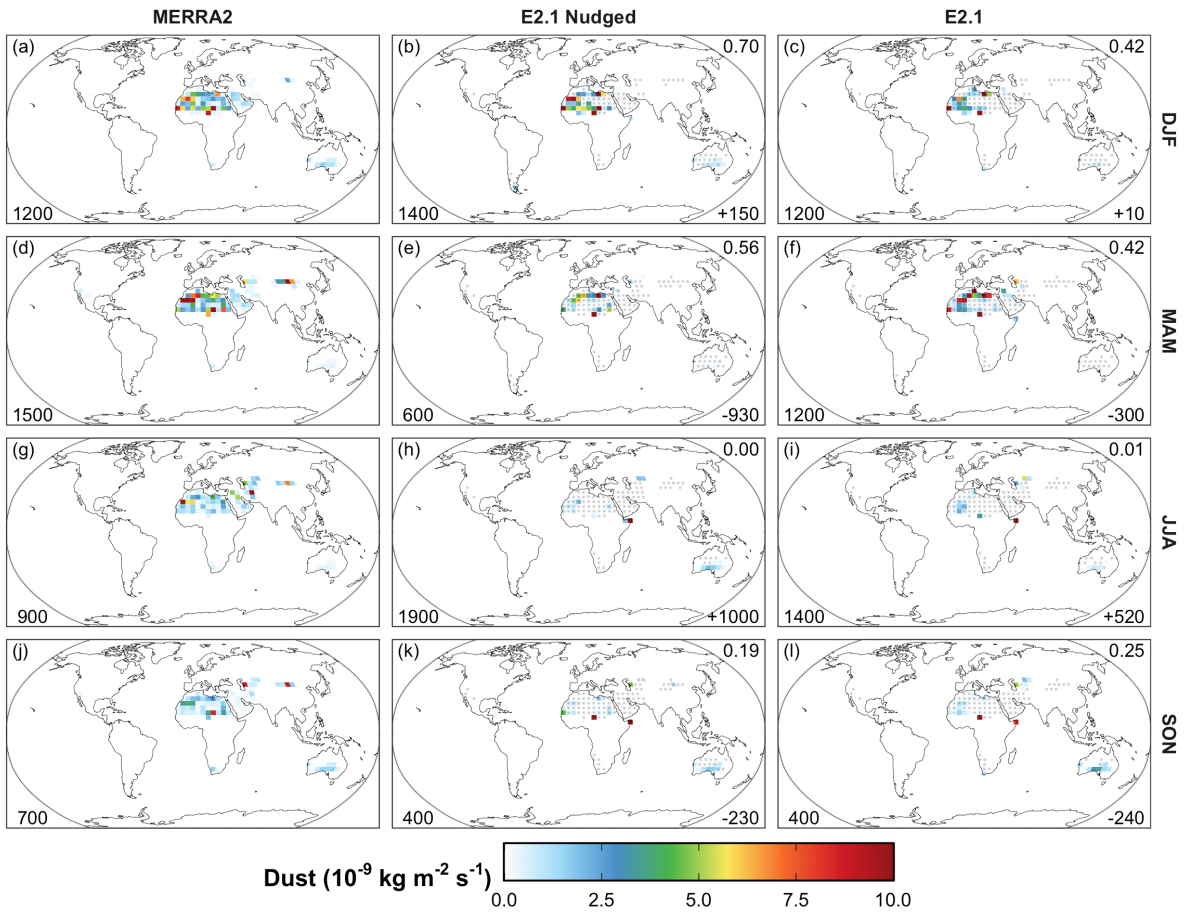
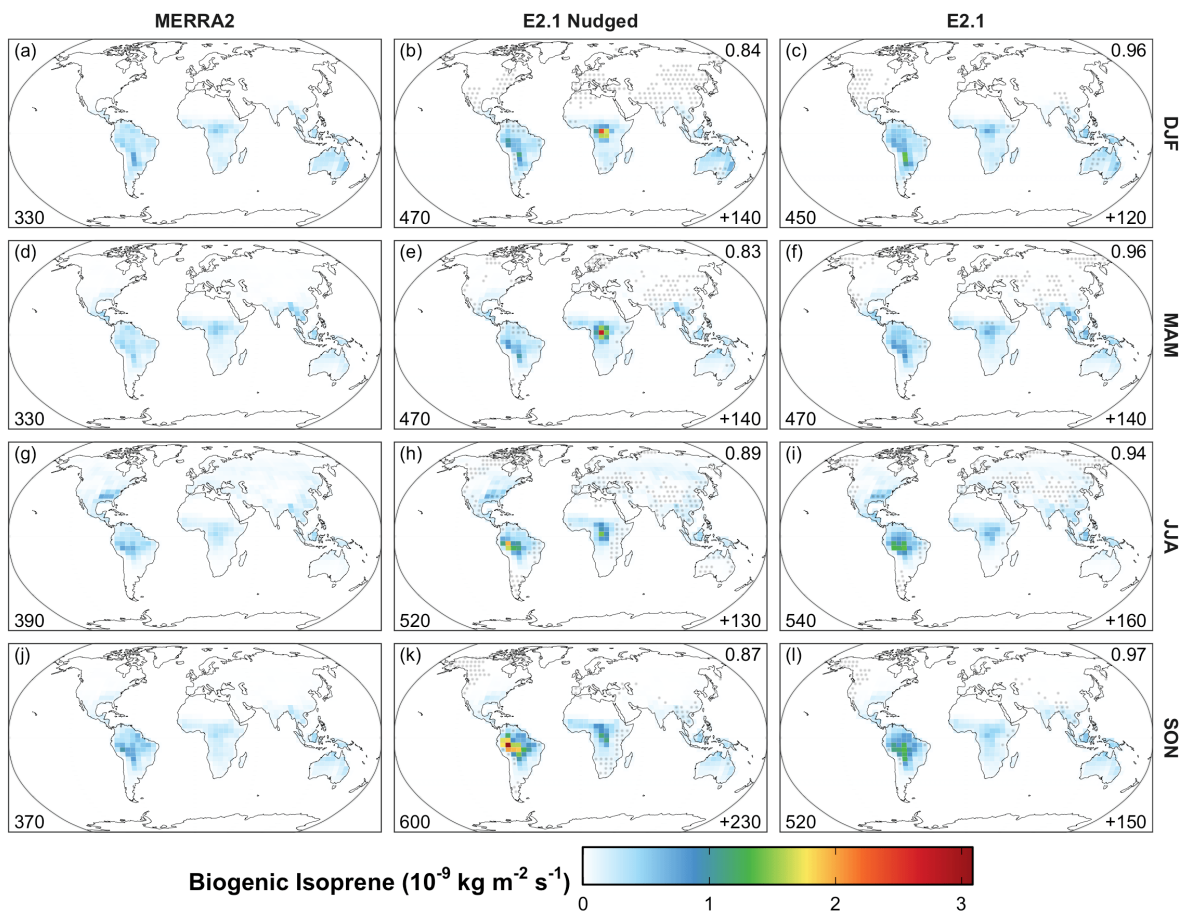
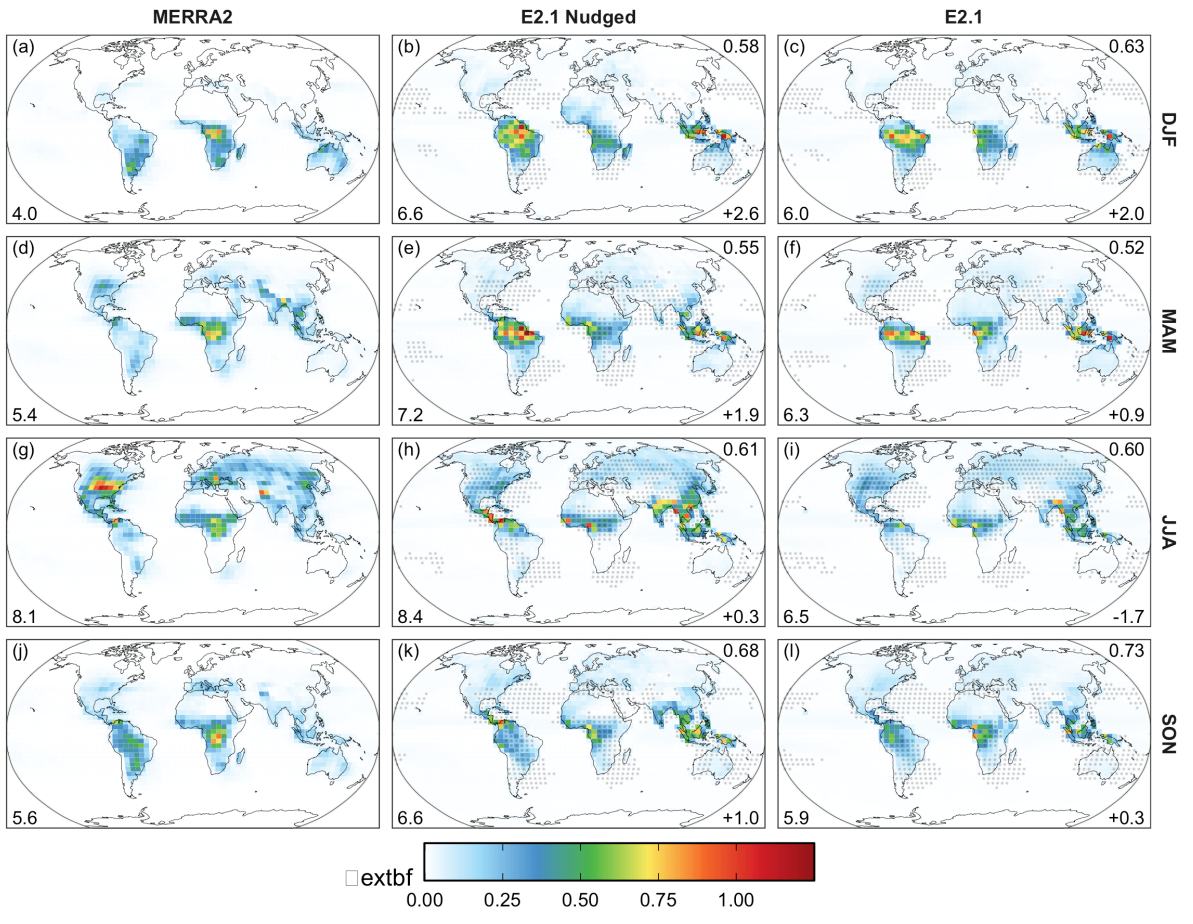


Figure S57: Same as Fig. S55, but for aeolian mineral dust emissions.



**Figure S58:** Same as **Fig. S55**, but for isoprene (2-methyl-1,3-butadiene;  $\text{CH}_2=\text{C}(\text{CH}_3)\text{CH}=\text{CH}_2$ ) from terrestrial plants.





**Figure S59:** Same as **Fig. S55**, but for vertically integrated columns of NO from lightning, and with global total units of  $\text{Tg N a}^{-1}$ .

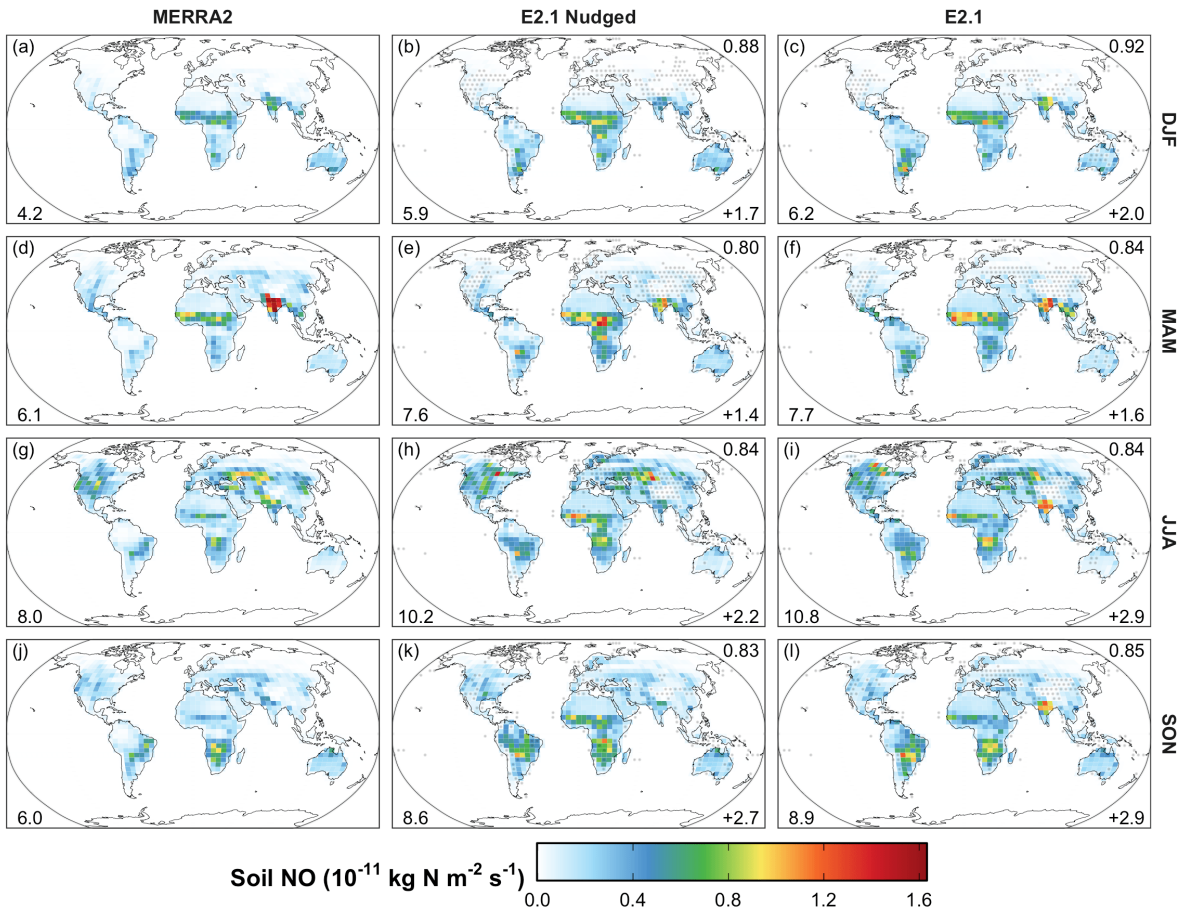
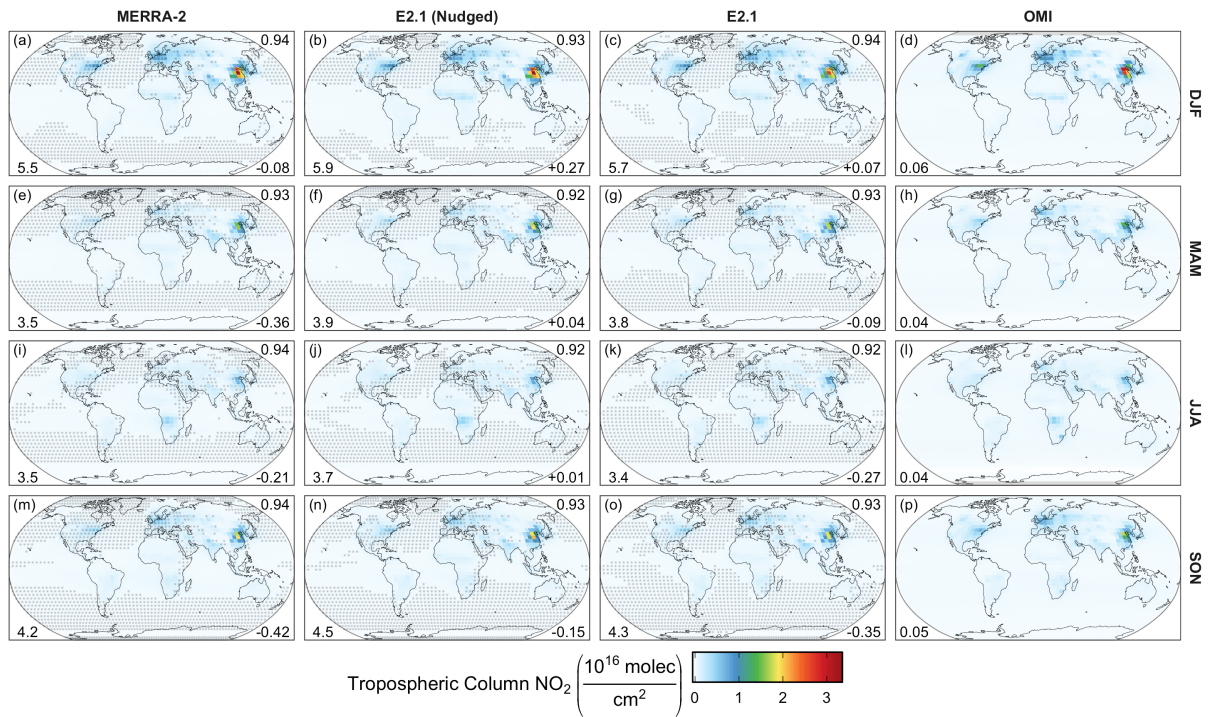
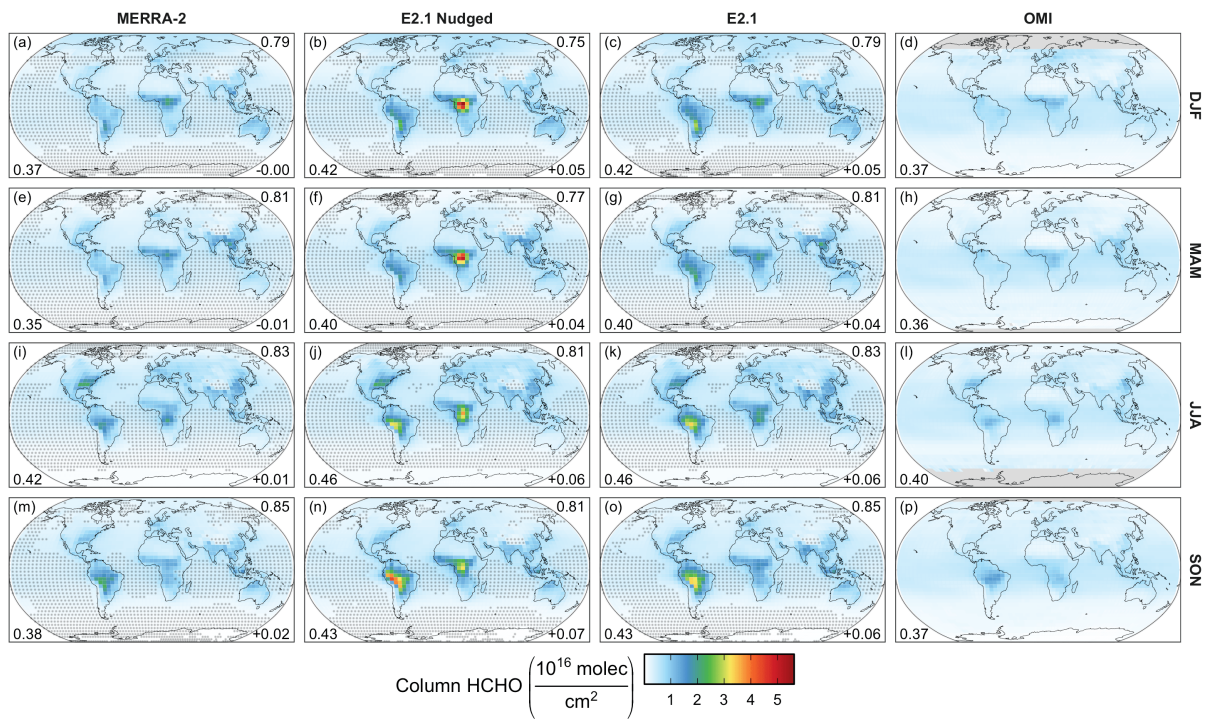


Figure S60: Same as Fig. S59, but for NO from soil microbial activity.

### S3 Evaluation



**Figure S61:** The same as panels a-d of Fig. 15 in the main text, but for each season.



**Figure S62:** The same as panels e-h of Fig. 15 in the main text, but for each season.



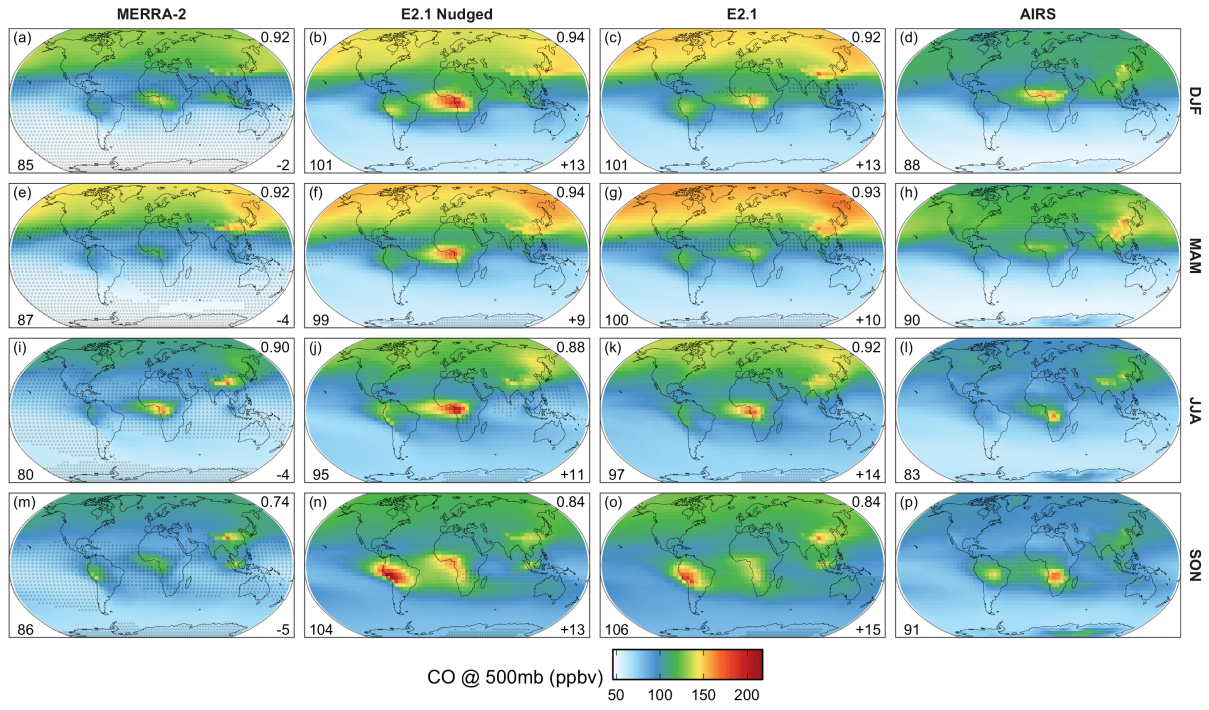


**Figure S63:** The same as panels i-l of Fig. 15 in the main text, but for each season.



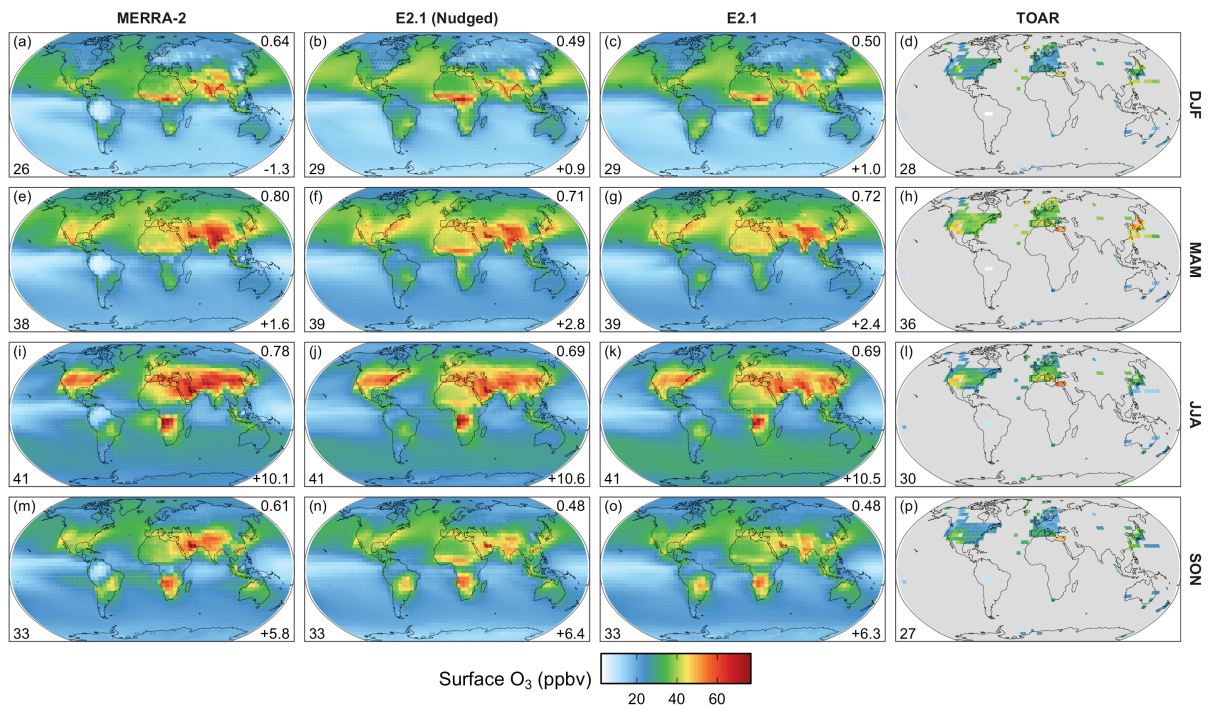


**Figure S64:** The same as panels a-d of Fig. 16 in the main text, but for each season.

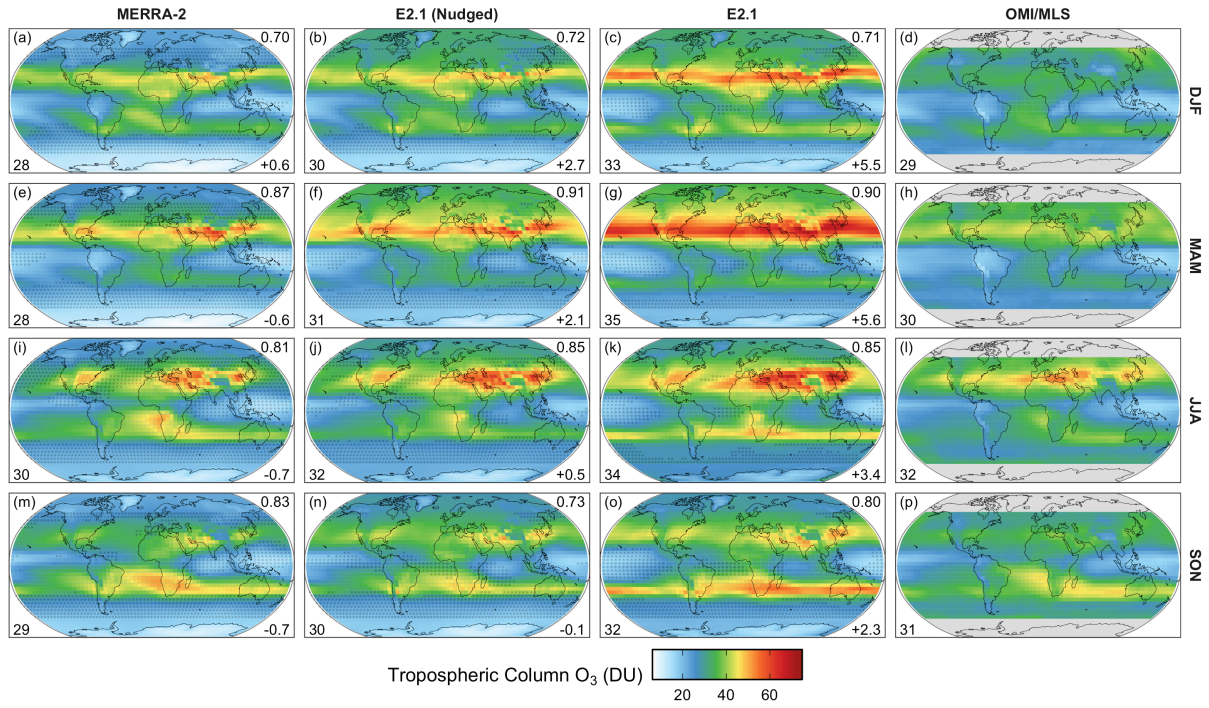


**Figure S65:** The same as panels e-h of Fig. 16 in the main text, but for each season.

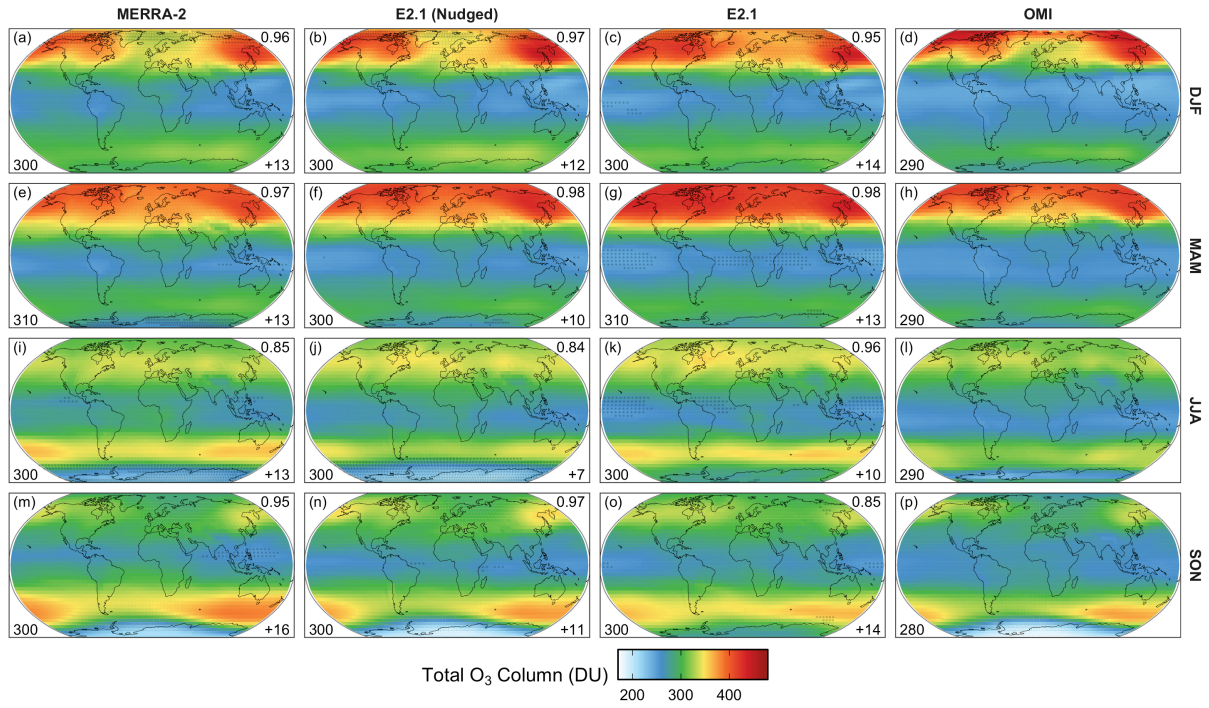


**Figure S66:** The same as panels i-l of Fig. 16 in the main text, but for each season.

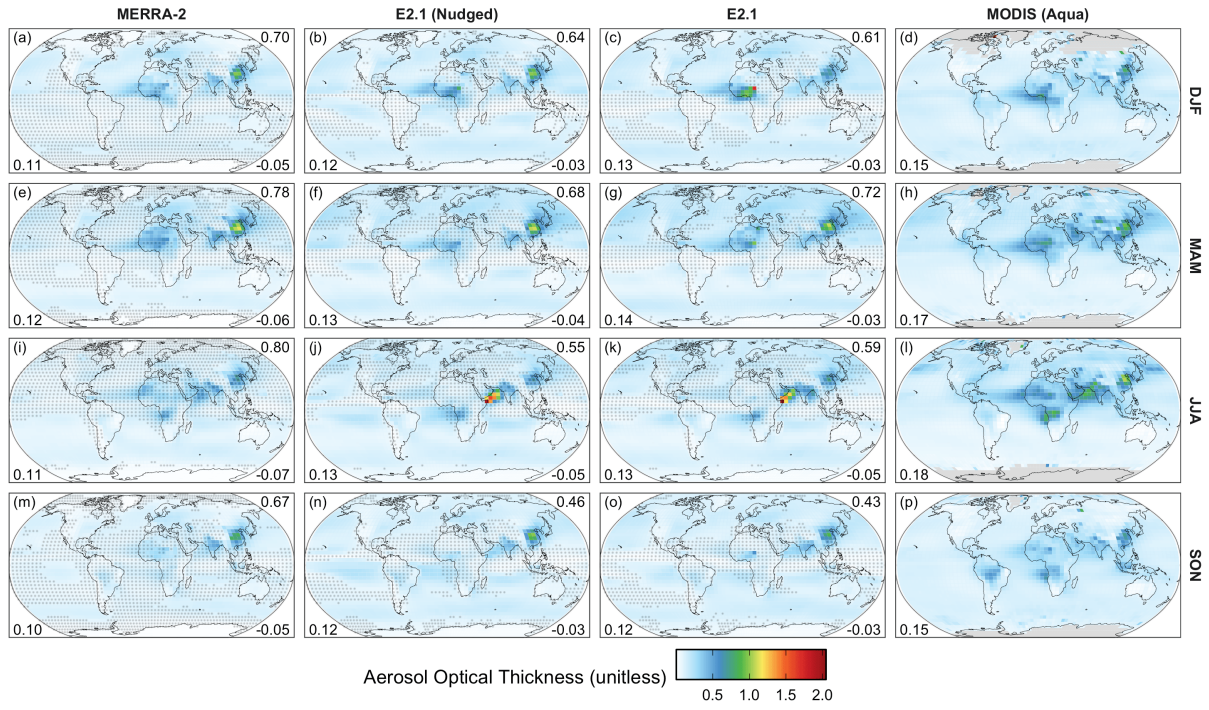


**Figure S67:** The same as panels e-h of Fig. 16 in the main text, but for each season.



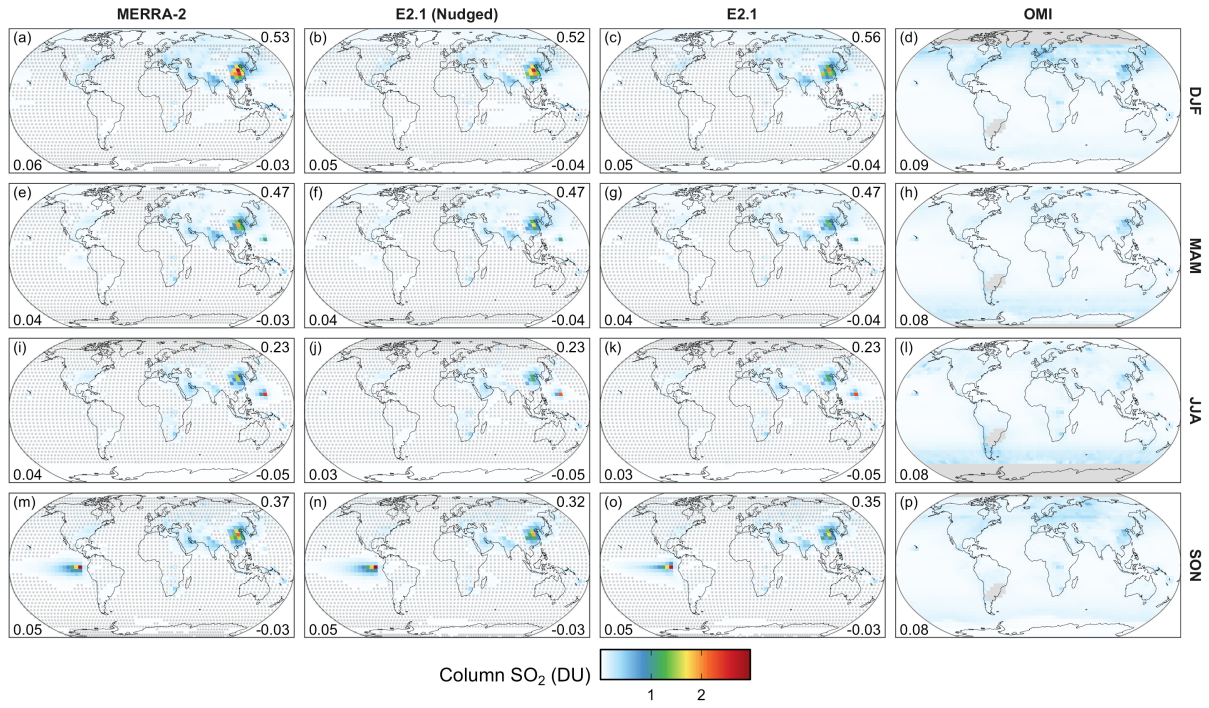


**Figure S68:** The same as panels i-l of Fig. 16 in the main text, but for each season.



## References

- Gelaro, R., McCarty, W., Suárez, M., Todling, R., Molod, A., Takacs, L., Randles, C., Darmenov, A., Bosilovich, M., Reichle, R., Wargan, K., Coy, L., Cullather, R., Draper, C., Akella, S., Buchard, V., Conaty, A., da Silva, A., Gu, W., Kim, G., Koster, R., Lucchesi, R., Merkova, D., Nielsen, J., Partyka, G., Pawson, S., Putman, W., Rienecker, M., Schubert, S., Sienkiewicz, M., and Zhao, B.: The Modern-Era Retrospective Analysis for Research and Applications, Version 2 (MERRA-2)., *J Climate*, Volume 30, 5419–5454, <https://doi.org/10.1175/JCLI-D-16-0758.1>, 2017.
- Gidden, M. J., Riahi, K., Smith, S. J., Fujimori, S., Luderer, G., Kriegler, E., van Vuuren, D. P., van den Berg, M., Feng, L., Klein, D., Calvin, K., Doelman, J. C., Frank, S., Fricko, O., Harm- sen, M., Hasegawa, T., Havlik, P., Hilaire, J., Hoesly, R., Horing, J., Popp, A., Stehfest, E., and Takahashi, K.: Global emissions pathways under different socioeconomic scenarios for use in CMIP6: a dataset of harmonized emissions trajectories through the end of the century, *Geosci- entific Model Development*, 12, 1443–1475, <https://doi.org/10.5194/gmd-12-1443-2019>, 2019.
- van Marle, M. J. E., Kloster, S., Magi, B. I., Marlon, J. R., Daniiau, A.-L., Field, R. D., Arneeth, A., Forrest, M., Hantson, S., Kehrwald, N. M., Knorr, W., Lasslop, G., Li, F., Mangeon, S., Yue, C., Kaiser, J. W., and van der Werf, G. R.: Historic global biomass burning emissions for CMIP6 (BB4CMIP) based on merging satellite observations with proxies and fire models (1750–2015), *Geoscientific Model Development*, 10, 3329–3357, <https://doi.org/10.5194/gmd-10-3329-2017>, 2017.